

Relaxing cosmological tensions with a sign switching cosmological constant

Özgür Akarsu^{1,*}, Suresh Kumar^{2,†}, Emre Özülker^{1,3,‡} and J. Alberto Vazquez^{4,§}

¹*Department of Physics, Istanbul Technical University, Maslak 34469, Istanbul, Turkey*

²*Department of Mathematics, Indira Gandhi University, Meerpur, Haryana-122502, India*

³*Aix Marseille Univ, Université de Toulon, CNRS, CPT, Marseille, France*

⁴*Instituto de Ciencias Físicas, Universidad Nacional Autónoma de México, Cuernavaca, Morelos 62210, México*

(Received 25 August 2021; accepted 19 October 2021)

Inspired by the recent conjecture that the Universe has recently transitioned from anti-de Sitter vacua to de Sitter vacua due to graduated dark energy, we extend the standard Λ CDM model by a cosmological constant (Λ_s) that switches sign at a certain redshift z_{\dagger} , and we call this model Λ_s CDM. We discuss the construction and theoretical features of this model in detail and find out that, when the consistency of the Λ_s CDM model with the cosmic microwave background (CMB) data is ensured, (i) $z_{\dagger} \gtrsim 1.1$ is implied by the condition that the Universe monotonically expands, (ii) H_0 and M_B (type Ia supernovae absolute magnitude) values are inversely correlated with z_{\dagger} and reach $H_0 \approx 74.5 \text{ km s}^{-1} \text{ Mpc}^{-1}$ and $M_B \approx -19.2 \text{ mag}$ for $z_{\dagger} = 1.5$, in agreement with the SHOES measurements, and (iii) $H(z)$ presents an excellent fit to the Ly- α measurements provided that $z_{\dagger} \lesssim 2.34$. We further investigate the model constraints by using the full *Planck* CMB data set, with and without baryon acoustic oscillation (BAO) data. We find that the CMB data alone does not constrain z_{\dagger} , but the CMB + BAO data set favors the sign switch of Λ_s , providing the constraint $z_{\dagger} = 2.44 \pm 0.29$ (68% C.L.). Our analysis reveals that the lower and upper limits of z_{\dagger} are controlled by the Galaxy and Ly- α BAO measurements, respectively, and the larger z_{\dagger} values imposed by the Galaxy BAO data prevent the model from achieving the highest local H_0 measurements. In general, the Λ_s CDM model (i) relaxes the H_0 tension while being fully consistent with the tip of the red giant branch measurements, (ii) relaxes the M_B tension, (iii) removes the discrepancy with the Ly- α measurements, (iv) relaxes the S_8 tension, and (v) finds a better agreement with the big bang nucleosynthesis constraints on the physical baryon density. We find no strong statistical evidence to discriminate between the Λ_s CDM and Λ CDM models. However, interesting and promising features of the Λ_s CDM model, which we describe in our study, provide an advantage over Λ CDM.

DOI:

I. INTRODUCTION

Over the last few years, there has been a growing consensus that the standard cosmological model—the so-called Lambda cold dark matter (Λ CDM) model—could in fact be an approximation to a more realistic one that still needs to be fully understood [1]. Phenomenologically, this new model is not expected to deviate drastically from Λ CDM, which is in excellent agreement with most of the currently available data [2–6]; however, it could be conceptually very different, and its deviations could be nontrivial. The recent developments, both theoretical (e.g., the de Sitter swampland conjecture [7–14]) and observational (e.g., the tensions hint at some unexpected and/or nontrivial deviations

from Λ CDM; see Refs. [15–66], and Refs. [67–70] for more references), along with the cosmological constant problems [71,72], suggest that attaining it would be an elusive task. These tensions are of great interest, not only in cosmology, but also in theoretical physics, as they could imply new physics beyond the well-established fundamental theories that underpin, and even extend, the Λ CDM model. The so-called H_0 tension—the deficit in the Hubble constant (H_0) predicted by the *Planck* cosmic microwave background (CMB) data within the Λ CDM model [6] when compared to its model-independent determinations from local measurements of distances and redshifts [73–79]—among others, is now described by many as a crisis. See Ref. [67] for a comprehensive list of references on the H_0 tension, and Ref. [80] for a recent comprehensive review, including a discussion of recent H_0 estimates and a summary of the proposed theoretical solutions. It has turned out to be a more challenging problem than originally thought as it worsens when the cosmological constant (Λ)

* akarsuo@itu.edu.tr

† suresh.math@igu.ac.in

‡ ozulker17@itu.edu.tr

§ javazquez@icf.unam.mx

is replaced by generic quintessence models of dark energy (DE), and is only partially relaxed when it is replaced by the simplest phantom (or quintom) models [32–36]. Notably, it was reported that the H_0 tension—as well as a number of other low-redshift discrepancies—could be alleviated by a dynamical DE that assumes negative or rapidly vanishing energy density values at high redshifts [16,37–61]. The fact that the *Planck* CMB data alone favors positive spatial curvature ($\Omega_{k0} < 0$), on top of the Λ CDM model, suggests that curvature might be the simplest explanation for a negative energy density source (effectively); however, the drastic exacerbation of the H_0 tension for the Λ CDM model with spatial curvature, and the favoring of spatial flatness ($\Omega_{k0} = 0$) with extremely high precision by the *Planck* CMB data in combination with other astrophysical data such as baryon acoustic oscillations (BAO) and cosmic chronometers, indicate that the negative energy source cannot be spatial curvature, but a nontrivially evolving DE [6,22–28].

The CMB power spectrum by itself, for a given cosmological model, provides powerful constraints on the Hubble parameter $H(z)$ at the background level once the comoving sound horizon at CMB last scattering, r_* , is given [80–82]. The comoving sound horizon at last scattering is determined entirely by the pre-recombination Universe, and is given by $r_* = \int_{z_*}^{\infty} c_s H^{-1} dz$, where c_s is the sound speed in the plasma and $z_* \approx 1100$ is the redshift of last scattering. The acoustic angular scale on the sky, θ_* , which is measured almost model independently with a precision of 0.03% [6], determines the comoving angular diameter distance to last scattering $D_M(z_*)$ through the relation $D_M(z_*) = r_*/\theta_*$. The measured CMB monopole temperature determines the radiation energy density, and the positions and heights of the angular peaks determine $\rho_c(z_*)$ and $\rho_b(z_*)$, where ρ is the energy density and the indices stand for CDM and baryonic matter, respectively. Assuming a flat space, $D_M(z_*) = c \int_0^{z_*} H^{-1} dz$, where c is the speed of light (unless it is mentioned explicitly, we will use $c = 1$); for Λ CDM, the constraints from the CMB along with this integral are enough to infer the value of Λ and hence the complete evolution of $H(z)$. These steps make it clear how phantom/quintom extensions of Λ CDM, for which Λ is replaced by a DE density typically decreasing and approaching zero with increasing redshift, increase H_0 . The decreased DE density at high redshifts corresponds to a lower $H(z)$ at those redshifts compared to Λ CDM. Since $D_M(z_*)$ is the same to very high precision for different DE models, the decreased $H(z)$ at higher redshifts should be compensated by an increased $H(z)$ at lower redshifts (and hence an increased H_0) in order to keep the integral describing $D_M(z_*)$ unaltered. This also explains why quintessence models exacerbate the H_0 tension: these models have a DE density that increases with redshift, so the above mechanism is reversed. Note that the DE density

is negligible in these models for $z > z_*$ as in Λ CDM, so r_* is not affected by the dynamical nature of the DE. Nevertheless, the simplest phantom/quintom models can only partially relieve the H_0 tension [32–36]; however, a DE density that attains negative values at high redshifts can amplify this mechanism to enhance H_0 even further. We recall that the above discussion relies on r_* being fixed among different models, in contrast to models that modify the sound horizon to alter $D_M(z_*)$ and hence H_0 , e.g., early dark energy (EDE) models [83].

On top of increasing $H(z)$ at low redshifts and hence the H_0 value, a lower $H(z)$ at large redshifts compared to the Λ CDM model can provide better agreement with the Ly- α BAO measurements at the effective redshift $z \sim 2.34$ [84,85], if the drop in the DE density is large enough at that redshift. Also, if the drop is rapid enough, it can cause a nonmonotonic behavior of $H(z)$ which is hard to achieve without relying on a negative DE density. Such a nonmonotonic behavior can provide an even better description of the Ly- α data, and was initially suggested by the BOSS Collaboration after the BOSS DR11 data [37] presented an approximately 2.5σ discrepancy with the best-fit Λ CDM model of *Planck* 2015 [5]. They have also reported, in a companion paper [16], that a positive cosmological constant is consistent with their data set for $z < 1$, while a negative DE density is preferred for $z > 1.6$, which led them to suggest a nonmonotonic behavior of $H(z)$ at $z \sim 2$. The *Planck* Collaboration (2018) [6] does not include the Ly- α measurements in their default BAO data compilation since for the Λ CDM model and its simple extensions, they do not provide significant constraints once the CMB and Galaxy BAO data are used, and they do not conform well with the rest of the data set within the framework of these models. They also quote from Ref. [37] that well-motivated extensions of Λ CDM that could provide a resolution to this discrepancy are hard to construct. Currently, the discrepancy of the Ly- α measurements with the *Planck* 2015 best-fit Λ CDM is reduced to a mild $\sim 1.7\sigma$ when the combination of the BOSS survey and its extended version eBOSS in the SDSS DR14 [84,85] is considered, and reduced even further to a $\sim 1.5\sigma$ tension when the final eBOSS (SDSS DR16) measurement, which combines all of the data from eBOSS and BOSS [86,87], is considered. We note, however, that since H_0 values predicted by Λ CDM are lower than the local measurements of H_0 while $H(z)$ values predicted by Λ CDM at $z \sim 2.34$ are greater than the Ly- α measurements of $H(z)$, simple and/or well-motivated extensions of Λ CDM addressing either one of these discrepancies typically tend to exacerbate the other. Therefore, it is conceivable that such models relaxing the H_0 tension will also typically suffer from a greater tension with the Ly- α measurements. It is intriguing to note that the Ly- α discrepancy has certain parallelisms with the so-called S_8 discrepancy (quantifying a discordance between the CMB and low-redshift probes, which

174 will be further elaborated in Sec. III), e.g., S_8 constraints
 175 based on Ly- α measurements are in agreement with the
 176 low-redshift probes [88], simple extensions of Λ CDM that
 177 reduce the H_0 tension typically worsen the S_8 discrepancy
 178 and vice versa [68], and the S_8 discrepancy has also
 179 weakened with the latest observations [89,90]. These
 180 facts seem to hint that a model addressing the H_0 and
 181 Ly- α tensions simultaneously may also address the S_8
 182 tension. With all of these in hand, a DE density that is
 183 consistent with a positive cosmological constant today but
 184 assumes negative values in the past is not indispensable,
 185 and yet it is worth further investigation as it has the
 186 potential to result in a better agreement with the existing
 187 observational data, including Ly- α , while addressing the
 188 H_0 tension too.

189 In this paper, we study a simple extension of the Λ CDM
 190 model for which a cosmological constant that yields a
 191 negative value in the past switches sign at a certain redshift
 192 z_{\dagger} to attain its current positive value and drives the observed
 193 acceleration; it will be dubbed Λ_s CDM. Although this sign
 194 switch results in discontinuities in various fundamental
 195 functions, e.g., in $H(z)$, it can be considered as an approxi-
 196 mation to a rapid transition in the (possibly effective) DE
 197 density. In fact, the sign-switching feature of the Λ_s CDM
 198 model was first suggested in Ref. [44] when their graduated
 199 dark energy (gDE) model appeared to prefer a very rapid
 200 transition in the DE density resembling a step function
 201 whose absolute value is almost constant away from the
 202 transition point. In Sec. II, we first motivate the Λ_s CDM
 203 model starting from the gDE, and then study its theoretical
 204 features. In Sec. III, we conduct a robust observational
 205 analysis of the model with the latest data, and we conclude
 206 in Sec. IV.

207 II. Λ_s CDM MODEL: SIGN-SWITCHING Λ

208 The positive cosmological constant assumption of the
 209 Λ CDM model was investigated via the gDE characterized
 210 by a minimal dynamical deviation from the null inertial
 211 mass density $q = 0$ (where $q \equiv \rho + p$) of the cosmo-
 212 **4** logical constant—or, the usual vacuum energy of the
 213 quantum field theory (QFT). This deviation is in the form
 214 $q \propto \rho^\lambda < 0$, for which, provided that the parameter $\lambda < 1$
 215 is the ratio of two odd integers, the energy density ρ
 216 dynamically takes negative values in the past [44]. During
 217 the transition from negative to positive energy density,
 218 there comes a redshift for which the energy density is null;
 219 this redshift will be denoted by z_{\dagger} in the present work, but
 220 note that it was denoted by z_* in Ref. [44]. gDE exhibits a
 221 wide variety of behaviors depending on λ , but it is of
 222 particular interest to us that for large negative values of λ ,
 223 it establishes a phenomenological model characterized by
 224 a smooth function that approximately describes a Λ that
 225 switches sign in the late Universe to become positive
 226 today. It was shown via the gDE that the joint

227 observational data, including but not limited to the
 228 *Planck* CMB and Ly- α BAO (BOSS DR11) data, suggest
 229 that the cosmological constant changed its sign at $z \approx 2.32$
 230 and triggered the late-time acceleration, the behavior of
 231 which alleviates the H_0 tension and the discrepancy with
 232 the Ly- α BAO measurements simultaneously. For large
 233 negative values of λ , it turns out that $\rho_{\text{gDE}}/3H_0^2 \approx 0.70$ for
 234 $0 \leq z \lesssim 2.32$, but its energy density switches sign rapidly
 235 at $z_{\dagger} \approx 2.32$ (this z_{\dagger} value is quite stable for $\lambda \lesssim -4$) and
 236 settles into a value $\rho_{\text{gDE}}/3H_0^2 \sim -0.70$ and remains there
 237 for $z_{\dagger} \gtrsim 2.32$; moreover, the larger the negative values of
 238 λ , the more ρ_{gDE} resembles a step function, and the better
 239 fit to the data. For arbitrarily large negative values of λ ,
 240 ρ_{gDE} indeed transforms into a step function centred at z_{\dagger}
 241 with two branches yielding opposite values about zero.
 242 It is easy to check that λ is responsible from the rapidity of
 243 the sign change of the energy density, and for the
 244 constraint $\lambda = -17.9 \pm 5.8$ obtained on it, the function
 245 $\rho_{\text{gDE}}(z)$ already closely resembles a step function.
 246 Thus, the gDE suggesting large negative values of λ
 247 when confronted with the observations can be interpreted
 248 as a hint at a cosmological constant that achieved its
 249 present-day positive value by switching sign at $z_{\dagger} \sim 2.3$,
 250 but was negative in the earlier Universe.

251 Some general constraints that are typically applied to
 252 classical sources, irrespective of a detailed description,
 253 give further confidence to the interpretation of the gDE as
 254 a hint at a sign-switching cosmological constant [91,92].
 255 Let us consider the gDE as an actual barotropic fluid,
 256 $p = p(\rho)$. In this case, although it behaves almost like a
 257 cosmological constant (in spite of the fact that its value
 258 switches sign at $z \approx 2.32$) throughout the history of the
 259 Universe, strictly speaking, it violates the weak energy
 260 condition, namely, the non-negativity conditions on the
 261 energy density, $\rho \geq 0$, for $z > z_{\dagger}$, and on the inertial mass
 262 density, $q \geq 0$, at any given time. Moreover, there are
 263 phases during which $c_s^2 \gg 1$ and $c_s^2 < 0$, i.e., gDE violates
 264 the condition $0 \leq c_s^2 \leq 1$ on the speed of sound of a
 265 barotropic fluid given by the adiabatic formula
 266 $c_s^2 = dp/d\rho$. The upper limit (causality limit) is a rigorous
 267 limit, and its violation means the abandonment of the
 268 theory of relativity. The lower limit applies to a stable
 269 situation, and if violated, the fluid is classically unstable
 270 against small perturbations of its background energy
 271 density—the so-called Laplacian (or gradient) instability.
 272 Indeed, phenomenological fluid models of DE are difficult
 273 to motivate, and adiabatic fluid models are typically
 274 unstable against perturbations, since c_s^2 is usually negative
 275 for $w = p/\rho < 0$. It is possible to evade this constraint in
 276 nonadiabatic fluids—such as canonical scalar field
 277 (quintessence or phantom fields) and string-theory-
 278 inspired tachyon fields, for which the effective speed of
 279 sound $c_{s\text{eff}}$ (which governs the growth of inhomogeneities

in the fluid) remains consistent with $0 \leq c_{s,\text{eff}}^2 \leq 1$ —in
 adiabatic fluids if w decreases sufficiently fast as the
 Universe expands (e.g., Chaplygin gas), and in multifluid
 models of DE (e.g., quintom field) constructed from the
 combination of such fluids [93]. However, unlike such
 sources, it seems unlikely to evade this constraint in gDE,
 especially given the observationally preferred values of its
 free parameters. On the other hand, whether it is positive
 or negative, a cosmological constant, which corresponds
 to the $\lambda \rightarrow -\infty$ limit of the gDE, is well behaved: $\rho = 0$
 and $c_s^2 = 0$ (it has no speed of sound, and thereby does not
 support classical fluctuations). Regarding the negativity of
 the corresponding energy density (when $z > z_+$), a neg-
 ative cosmological constant is not only ubiquitous in the
 fundamental theoretical physics without any complica-
 tion, but also a theoretical sweet spot; an anti-de Sitter
 (AdS) background (provided by $\Lambda < 0$) is welcome due to
 the celebrated AdS/CFT correspondence [94] and is
 preferred by string theory and string-theory-motivated
 supergravities [95]. It is the positive cosmological con-
 stant that in fact suffers from theoretical challenges:
 getting a vacuum solution with a positive cosmological
 constant within string theory or formulating QFT on the
 background of a dS space (provided by $\Lambda > 0$) has been a
 notoriously difficult task [see Refs. [7,96–102]; addition-
 ally, see Refs. [11,103] for a recent review on models of
 the accelerating Universe (viz., for different mechanisms
 to obtain dS space/vacua and building models of quintes-
 sence) in supergravity and string theory]. Therefore, an
 approach that asserts that a positive-valued cosmological
 constant exists only in the late Universe (say, when
 $z \lesssim 2.3$) would enjoy limiting such difficulties to the late
 Universe. Of course, it is necessary to further study
 whether such an approach—say, transitions from an
 AdS background to a dS one—would be viable both
 theoretically and observationally (we further comment on
 such transitions in Sec. IV). Besides, studies considering
 the presence of a negative cosmological constant in
 various contexts are already plentiful in the cosmology
 literature. In the context of the inflationary Universe, see,
 e.g., Refs. [104–106] which considered inflation with
 multiple AdS vacua, and Ref. [107] which considered a
 cosmological constant that slowly varies from a positive
 value to a negative value and becomes vanishingly small
 at the end of inflation. In the context of EDE models,
 see, e.g., Ref. [55] which suggested the presence of AdS
 vacua around recombination to alleviate the H_0 tension,
 and the follow-up study in Ref. [56] which presented an
 α -attractor AdS model of EDE for which the AdS vacua
 originate from UV-complete theories in the cosmological
 setup with varying AdS depth. In the context of post-
 recombination modifications to the Λ CDM model, see,
 e.g., Refs. [38,40–47] which suggested that the cosmo-
 logical data prefer or are fully consistent with the pre-
 sence of a negative-valued cosmological constant at high

redshifts; some of these examples explicitly pronounce **5** 335
 the redshift scales $z \gtrsim 2.3$. Let us also mention that a 336
 negative (but not necessarily constant) effective energy 337
 component appears and finds applications in the cos- 338
 mology literature [see, e.g., scalar-tensor theories of 339
 gravity such as Brans-Dicke theory [108–112], as well 340
 as modified theories of gravity such as $f(R, \mathcal{L}_m)$ [113], 341
 $f(R, T)$ [114], $f(R, T_{\mu\nu}T^{\mu\nu})$ [115–120], Rastall gravity 342
 [59], and quadratic bimetric gravity [40]; theories in 343
 which Λ relaxes from a large initial value via an adjust- 344
 ment mechanism [121–123]; cosmological models 345
 based on Gauss-Bonnet gravity [124]; braneworld models 346
 [125,126]; higher-dimensional cosmologies that accom- 347
 modate dynamical reduction of the internal space 348
 [127–131]; a negative dark radiation component [132]; 349
 missing matter [29]; a dynamical $\Lambda(t)$ term [133]; phe- 350
 nomenological generalizations of the null inertial mass 351
 density of the usual vacuum energy [28,44,134–136]; a 352
 negative matter action [137–139]; and ghost-matter cos- 353
 mologies [140]]. 354

Thus, bringing all of these points together, it is 355
 tempting to consider the possibility that the cosmological 356
 constant switched sign and became positive in the late 357
 Universe, which then eventually started the acceleration. 358
 Accordingly, we introduce the Λ_s CDM model phenom- 359
 enologically, constructed simply by replacing the usual 360
 cosmological constant (Λ) of the standard Λ CDM model 361
 with a cosmological constant (Λ_s) that switches its sign 362
 from negative to positive when the Universe reaches a 363
 certain energy scale (redshift z_+) during its expansion, 364

$$\Lambda \rightarrow \Lambda_s \equiv \Lambda_{s0} \text{sgn}[z_+ - z], \quad (1)$$

where $\Lambda_{s0} > 0$. Here “sgn” is the signum function that 366
 reads $\text{sgn}[x] = -1, 0, 1$ for $x < 0$, $x = 0$, and $x > 0$, 367
 respectively. Accordingly, the Friedmann equation for the 368
 Λ_s CDM model reads 369

$$\frac{H^2}{H_0^2} = \Omega_{r0}(1+z)^4 + \Omega_{m0}(1+z)^3 + \Omega_{\Lambda_s0} \text{sgn}[z_+ - z], \quad (2)$$

where we consider the usual cosmological fluids [CDM (c) 370
 and baryons (b) described by the equations of state 372
 $w_c = w_b = 0$, and radiation (r), consisting of photons (γ) 373
 and neutrinos (ν), described by $w_r = \frac{1}{3}$] and $\Omega_{m0} + \Omega_{r0} +$ 374
 $\Omega_{\Lambda_s0} = 1$, with $\Omega_{m0} = \Omega_{c0} + \Omega_{b0}$. We define the 375
 present-day density parameters as $\Omega_{r0} = 8\pi G\rho_{r0}/(3H_0^2)$, 376
 $\Omega_{m0} = 8\pi G\rho_{m0}/(3H_0^2)$, and $\Omega_{\Lambda_s0} = \Lambda_{s0}/(3H_0^2)$. Note that 377
 the index 0 stands for the present-day values, but we 378
 will drop it from the indices of the density param- 379
 eters in the next section to avoid cluttered notation. 380
 Accordingly, the corresponding energy density and pres- 381
 sure for the dark energy read $\rho_{\text{DE}} = \Lambda_{s0} \text{sgn}[z_+ - z]/(8\pi G)$ 382
 and $p_{\text{DE}} = -\Lambda_{s0} \text{sgn}[z_+ - z]/(8\pi G)$, respectively, satisfy- 383
 ing the equation of state $p_{\text{DE}} = -\rho_{\text{DE}}$ like the usual 384

385 vacuum energy.¹ The radiation density parameter today is
 386 given by $\Omega_{r0} = 2.469 \times 10^{-5} h^{-2} (1 + 0.2271 N_{\text{eff}})$, where
 387 $h = H_0/100 \text{ km s}^{-1} \text{ Mpc}^{-1}$ is the dimensionless reduced
 388 Hubble constant and $N_{\text{eff}} = 3.046$ is the standard number
 389 of effective neutrino species with minimum allowed mass
 390 $m_\nu = 0.06 \text{ eV}$, as the present-day photon energy density is
 391 already extremely well constrained by the absolute
 392 CMB monopole temperature measured by FIRAS, $T_0 =$
 393 $2.7255 \pm 0.0006 \text{ K}$ [141].

394 To better understand the behavior of the Λ_s CDM model
 395 described by the Friedmann equation in Eq. (2), we
 396 proceed with giving the evolution of the scale factor in
 397 cosmic (proper) time t , i.e., $a(t)$, under the assumption that
 398 while the cosmological constant is positive ($\Lambda_s > 0$) the
 399 Universe always expands.² When radiation dominates
 400 the Friedmann equation (2), i.e., at redshifts larger than
 401 the matter-radiation equality, $z > z_{\text{eq}}$, like Λ CDM, Λ_s CDM
 402 is also well described by the Tolman model, viz., $a(t) \propto t^{\frac{1}{2}}$.
 403 On the other hand, when the radiation is negligible, i.e.,
 404 for $z > z_{\text{eq}}$, like Λ CDM, Λ_s CDM is also the Friedmann-
 405 Lemaître model (see, e.g., Ref. [142]), but with the
 406 exception that the cosmological constant switches
 407 sign at a certain time t_\dagger . For both of the models, the
 408 redshift of the matter-radiation equality is given by
 409 $1 + z_{\text{eq}} = 2.38 \times 10^4 \Omega_{m0} h^2$. For the Λ CDM model,
 410 $a_{\text{eq}}/a_0 \sim 3 \times 10^{-4}$ (as $z_{\text{eq}} \sim 3450$ [6]), which corresponds
 411 to $t_{\text{eq}} = \int_0^{a_{\text{eq}}} (aH)^{-1} da \sim 5 \times 10^4 \text{ yr}$. Note that these are
 412 negligibly small compared to the present age ($t_0 \sim$
 413 13.8 Gyr [6]) and size (a_0) of the Universe, and it is
 414 conceivable that this would not change in a viable cosmo-
 415 logical model based on Λ_s CDM. Therefore, for our
 416 purposes in this section, it will suffice to proceed below
 417 by ignoring radiation, namely, by constructing the scale
 418 factor of the Λ_s CDM model by gluing (at $t = t_\dagger$) the scale
 419 factor of the Friedmann-Lemaître model, whose cosmo-
 420 logical constant is negative (for $t < t_\dagger$), to the one whose
 421 cosmological constant is positive (for $t > t_\dagger$). Accordingly,
 422 the evolution of the scale factor in the Λ_s CDM model reads

¹Note that the signum function implies $p_{\text{DE}}(z_\dagger) = -\rho_{\text{DE}}(z_\dagger) = 0$;
 however, this is an artifact of using the signum function to
 describe the sign switch, and is not fundamental to the model.
 We could instead make use of, e.g., the Heaviside step function
 which is devoid of this artifact, but this would make no
 meaningful contribution to our discussions, and would crowd
 the equations; for this reason, we stick with the familiar signum
 function. Furthermore, Λ_s CDM can also be extended by
 modeling the sign switch with smooth sigmoid functions which
 would allow one to also study the rapidity of the transition, but
 we leave this possibility to future works.

²In the case where the Universe starts contracting before the
 cosmological constant switches sign to become positive, one
 naturally expects the positive cosmological constant to cause an
 expansion after the switch; however, the resumption of the
 contraction after the sign switch is a mathematically viable
 alternative that we do not investigate in this paper due to the
 clear evidence in favor of the present-day expansion.

$$a(t) = \begin{cases} A^{\frac{1}{3}} \sin^{\frac{2}{3}} \left(\frac{3}{2} \sqrt{\frac{\Lambda_{s0}}{3}} t \right) & \text{for } t \leq t_\dagger, \\ A^{\frac{1}{3}} \sinh^{\frac{2}{3}} \left[\frac{3}{2} \left(\sqrt{\frac{\Lambda_{s0}}{3}} t + B \right) \right] & \text{for } t \geq t_\dagger, \end{cases} \quad (3)$$

where

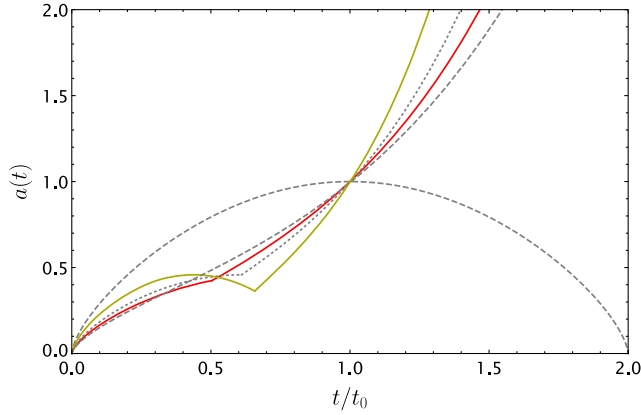
$$A = \sinh^{-2} \left[\frac{3}{2} \left(\sqrt{\frac{\Lambda_{s0}}{3}} t_0 + B \right) \right],$$

$$B = \operatorname{arcsinh} \left[\sin \left(\frac{3}{2} \sqrt{\frac{\Lambda_{s0}}{3}} t_\dagger \right) - \frac{3}{2} \sqrt{\frac{\Lambda_{s0}}{3}} t_\dagger \right], \quad (4)$$

and $t_\dagger < 2\pi/\sqrt{3\Lambda_{s0}}$ to ensure $a(t) > 0$ for $t > 0$. To derive
 this solution, we have normalized the scale factor such that
 $a(t_0) = 1$ (with t_0 being the cosmic time today), and
 introduced the initial condition $a(0) = 0$ (i.e., assumed
 that the Universe started with a big bang, and used a time
 parametrization such that the big bang was at $t = 0$, which
 also results in t_0 being the age of the Universe today). Note
 that, under these boundary conditions, general relativity
 implies, through the Friedmann equations, that this solution
 satisfies $A = 8\pi G \rho_{m0}/\Lambda_{s0}$, which also determines the age
 of the Universe today for a given ρ_{m0} and Λ_{s0} using Eq. (4).
 The assumption of an ever-expanding Universe ($H > 0$)
 implies the condition $t_\dagger < \pi/\sqrt{3\Lambda_{s0}}$, as the cosmological
 constant must switch to its present-day positive value
 before (in time) the maximum of the sine function is
 reached. Figure 1 illustrates five qualitatively different
 scenarios that vary based on t_\dagger . The condition for the
 ever-expanding Universe, after being used in Eq. (3) to find
 the maximum value possible for $a(t_\dagger) = 1/(1 + z_\dagger)$, trans-
 lates into the following condition on z_\dagger :

$$z_\dagger > \left(\frac{\Omega_{\Lambda_s 0}}{1 - \Omega_{\Lambda_s 0}} \right)^{\frac{1}{3}} - 1. \quad (5)$$

Note that Eq. (5) can also be easily obtained from Eq. (2) by
 enforcing $H > 0$ for all redshift values once the radiation
 density parameter is neglected. If this condition is violated,
 the Universe enters a contracting phase due to the negative
 cosmological constant until it switches sign to become
 positive, which then either restarts the expansion and
 eventually results in the accelerated expansion of the
 Universe (dark yellow curve in Fig. 1) or further assists
 the contraction and causes the Universe to recollapse (not
 present in Fig. 1). An effect worth noting for the dark
 yellow curve in Fig. 1 is that the one-to-one correspondence
 between redshift and cosmic time is broken; hence,
 observations from the same redshift can correspond to
 signals coming from two different times. We do not
 elaborate on the possibility of these interesting scenarios
 in the present work. Therefore, in what follows we proceed
 under the condition of an ever-expanding Universe, which,
 for instance, gives $z_\dagger > 0.33$ for $\Omega_{\Lambda_s 0} = 0.7$.



F1:1 FIG. 1. Evolution of the scale factor for various scenarios under
 F1:2 the constraints $a(0) = 0$ and $a(t_0) = 1$. The dashed gray curves
 F1:3 are the edge cases $t_{\dagger} = 0$ and $t_{\dagger} \rightarrow \infty$, i.e., the standard
 F1:4 Friedmann-Lemaître models for a positive cosmological constant
 F1:5 (which expands forever) and for a negative cosmological constant
 F1:6 (which recollapses), respectively. The red curve corresponds to an
 F1:7 ever-expanding Universe, i.e., $t_{\dagger} < \pi/\sqrt{3\Lambda_{s0}}$, and is the most
 F1:8 relevant case for this paper. The dark yellow curve is for
 F1:9 $t_{\dagger} > \pi/\sqrt{3\Lambda_{s0}}$, and the dotted gray curve is the critical case
 F1:10 $t_{\dagger} = \pi/\sqrt{3\Lambda_{s0}}$. Note that radiation is neglected in the figure, but
 F1:11 since $t_{\text{eq}}/t_0 \approx 0$ and $a(t_{\text{eq}}) \approx 0$, its inclusion would not result in
 F1:12 visible changes.

465 The deceleration parameter ($q \equiv -\frac{\ddot{a}}{aH^2}$, where a dot
 466 denotes d/dt) for the Λ_s CDM model can simply be written
 467 as

$$q = -1 + \frac{3}{2} \left[\frac{\Omega_{\Lambda_s0} \text{sgn}[z_{\dagger} - z]}{1 - \Omega_{\Lambda_s0} \text{sgn}[z_{\dagger} - z]} (1+z)^{-3} + 1 \right]^{-1}, \quad (6)$$

469 where we have neglected radiation. For $z > z_{\dagger}$, it evolves
 470 from $q = \frac{1}{2}$ during the matter-dominated epoch toward
 471 $q = 2$ as the negative cosmological constant dominates
 472 with the expansion of the Universe. This equation is solved
 473 for $q(z_c) = 0$ only when $z < z_{\dagger}$, and the solution reads

$$z_c = 2^{\frac{1}{3}} \left(\frac{\Omega_{\Lambda_s0}}{1 - \Omega_{\Lambda_s0}} \right)^{\frac{1}{3}} - 1, \quad (7)$$

475 provided that $z_c < z_{\dagger}$. For the Λ CDM model, z_c is the
 476 redshift at which the Universe enters its accelerated
 477 phase since its smoothly varying deceleration parameter
 478 should pass through the point $q(z_c) = 0$ before becoming
 479 negative. For Λ_s CDM, however, due to the discontinuous
 480 features of the model, its deceleration parameter does not
 481 need to attain the value $q = 0$ in order to transit to the
 482 accelerated phase from the decelerated phase. While z_c
 483 defines the redshift at the beginning of the acceleration
 484 if $z_c < z_{\dagger}$, if $z_{\dagger} < z_c$, $q = 0$ is never satisfied and the
 485 deceleration parameter jumps from positive to negative
 486 values at z_{\dagger} which marks the beginning of acceleration in

this case (see the dotted gray curve in Fig. 5 for an example, 487
 and see Sec. II A for relevant definitions). For example, for 488
 $\Omega_{\Lambda_s0} = 0.7$, in the very extreme case $z_{\dagger} = 0.33$ allowed by 489
 Eq. (5), q jumps from ≈ 0.82 to ≈ -0.25 at z_{\dagger} , and the 490
 acceleration is onset. Also, the jerk parameter ($j \equiv \frac{\ddot{a}}{aH^3}$) is 491
 undefined at the single point $z = z_{\dagger}$; however, one may 492
 check that, when radiation is neglected, both the Λ CDM 493
 and Λ_s CDM models yield $j = 1$ everywhere that it is 494
 defined throughout the history of the Universe. Note that if 495
 one considers the sign-switch feature of Λ_s CDM as an 496
 approximation to a DE density that very rapidly yet 497
 smoothly transitions from negative to positive, q is not 498
 discontinuous and j is not undefined at any point; instead, 499
 q goes through a smooth but very sharp transition [e.g., 500
 from $q(0.35) \approx 0.8$ to $q(0.33) \approx -0.25$], and $j \gg 1$ during 501
 this short transition period while it is again unity (or almost 502
 unity) anywhere else. 503

A. Analyzing the parameter z_{\dagger} , and its effects on some cosmological tensions

504 The deviations of the Λ_s CDM model from the Λ CDM 505
 model are controlled by its additional parameter z_{\dagger} . Before 506
 directly confronting the model with observational data 507
 in the next section, here we attempt to assess the range 508
 and effects of z_{\dagger} . We notice that Λ_s CDM is exactly 509
 the same as Λ CDM at redshifts lower than z_{\dagger} given 510
 that $(\Omega_{m0}h^2)_{\Lambda_s\text{CDM}} = (\Omega_{m0}h^2)_{\Lambda\text{CDM}}$ and $\Lambda_{s0} = \Lambda$, while 511
 these two models differ at redshifts larger than z_{\dagger} as 512
 $\Lambda_s(z > z_{\dagger}) = -\Lambda_{s0}$ in Λ_s CDM, yet this difference 513
 disappears once again at even larger redshifts, as the 514
 corresponding density parameters, $\Omega_{\Lambda_s} = \Lambda_s/(3H^2)$ and 515
 $\Omega_{\Lambda} = \Lambda/(3H^2)$, regardless of whether they yield positive 516
 or negative values, rapidly become negligible with increas- 517
 ing redshift in both models. Thus, Λ_s CDM differs from 518
 Λ CDM for $z_{\dagger} < z \ll z_*$; hence, it is, in practice, a post- 519
 recombination modification to Λ CDM. However, note that 520
 the abrupt-change feature of $H(z)$ in Λ_s CDM (or of the 521
 models that are well approximated by such as the gDE) 522
 would not be captured by the spline reconstruction of the 523
 Hubble parameter in Refs. [82,143,144]; hence, it evades 524
 their arguments against post-recombination deviations 525
 from Λ CDM, and furthermore, since $j(z) = 1$ (neglecting 526
 radiation) and we expect $q_0 \sim -0.55$ at $z \sim 0$ for Λ_s CDM 527
 as in Λ CDM, a direct comparison of its H_0 value with the 528
 SH0ES Collaboration measurements of H_0 [73,75] should 529
 not be an issue, unlike in models with rapidly changing 530
 $H(z)$ values for $z \lesssim 0.1$ [145,146]. The SH0ES H_0 deter- 531
 mination is a two-step process: first, anchors, Cepheids, 532
 and calibrators are combined to produce a constraint 533
 on the type Ia supernovae (SnIa) absolute magnitude 534
 M_B , and second, Hubble-flow SnIa data are used to probe 535
 the luminosity distance–redshift relation in order to deter- 536
 mine H_0 by adopting a cosmography with $q_0 = -0.55$ and 537
 538

539 $j_0 = 1$ [73] (small deviations from $q_0 = -0.55$ have an
 540 insignificant effect on the determined H_0 value [76,146]).
 541 These suggest that, as Λ_s CDM yields $q_0 \sim -0.55$ (see
 542 Fig. 5) and $j_0 = 1$, it respects the methodology used by the
 543 SH0ES Collaboration to obtain M_B and H_0 ; thus, if
 544 Λ_s CDM is to resolve the SH0ES H_0 tension, it is
 545 conceivable that it will also be in good agreement with
 546 the SH0ES M_B measurement [146,147].

547 We now analyze the parameter z_{\dagger} with respect to the H_0 ,
 548 Ly- α , and Galaxy BAO measurements while the consistency
 549 with the CMB data is ensured. To do so, we fix the comoving
 550 angular diameter distance to last scattering, $D_M(z_*)$, to
 551 that of Λ CDM for Λ_s CDM (we assume $z_* = 1100$
 552 for both models). This is a good guiding principle since
 553 once the sound horizon at CMB last scattering, r_* , is
 554 given, $D_M(z_*)$ is very strictly constrained in an almost
 555 model-independent way by the measurement of the angular
 556 acoustic scale θ_* since $D_M(z_*) = r_*/\theta_*$. And, for Λ_s CDM,
 557 we expect almost no deviations in the pre-recombination
 558 dynamics of the Universe, and hence in r_* , once we fix its
 559 $\rho_m(z_*)$ and $\rho_r(z_*)$ values to those of Λ CDM. Fixing $\rho_m(z_*)$
 560 in this way is well justified as this value is very well
 561 constrained by the relative heights of the CMB power
 562 spectra peaks, and its corresponding baryon density is in
 563 good agreement with standard big bang nucleosynthesis
 564 (BBN), providing even more confidence. Since $\rho_r(z_*)$ is also
 565 fixed by the CMB monopole temperature measurements, the
 566 only difference regarding the pre-recombination dynamics
 567 would be due to the difference between the values of Λ_s in
 568 Λ_s CDM and Λ in Λ CDM, but, since these have negligible
 569 corresponding energy densities for $z \geq z_*$, r_* is not signifi-
 570 cantly affected. We fix $z_* = 1100$ simply because it is a
 571 reasonable choice and we do not expect it to affect our
 572 argumentation since the relevant integrals are not substan-
 573 tially affected by its sensible deviations. After we fix
 574 $D_M(z_*)$ in this way, we can calculate Λ_{s0} using the equality
 575 $D_M(z) = c \int_0^z H^{-1}(z') dz'$ for the comoving angular dia-
 576 meter distance at z , which is satisfied for the spatially flat
 577 Robertson-Walker (RW) metric. Knowing Λ_{s0} , ρ_m , and ρ_r at
 578 a single point allows us to construct $H(z)$ at all times and
 579 discuss how z_{\dagger} modifies $H(z)$ and H_0 with respect to
 580 observations using visualization methods similar to those
 581 of Ref. [16].

582 This construction is done in Figs. 2 and 3 based on the
 583 results of *Planck* 2018 [6] (see the figure captions for more
 584 details) but neglecting the radiation energy density. It is
 585 seen from Fig. 2 that Λ_s CDM attains greater values of H_0
 586 compared to Λ CDM, and z_{\dagger} is inversely correlated with H_0 .
 587 Such greater values are a direct consequence of the sudden
 588 drop in $H(z)$ due to the negative cosmological constant for
 589 $z > z_{\dagger}$, as explained in the Introduction. Additionally, as
 590 seen in the top panel of Fig. 3, the drop in $H(z)$ due to the
 591 sign switch allows Λ_s CDM to better agree with the Ly- α
 592 data; however, this amelioration of the Ly- α discrepancy
 593 disappears immediately for $z_{\dagger} \gtrsim 2.4$. Moreover, as z_{\dagger}

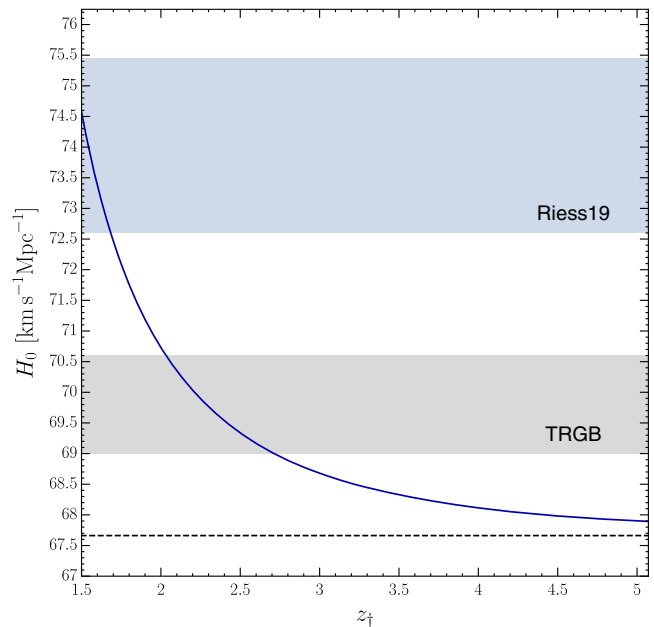
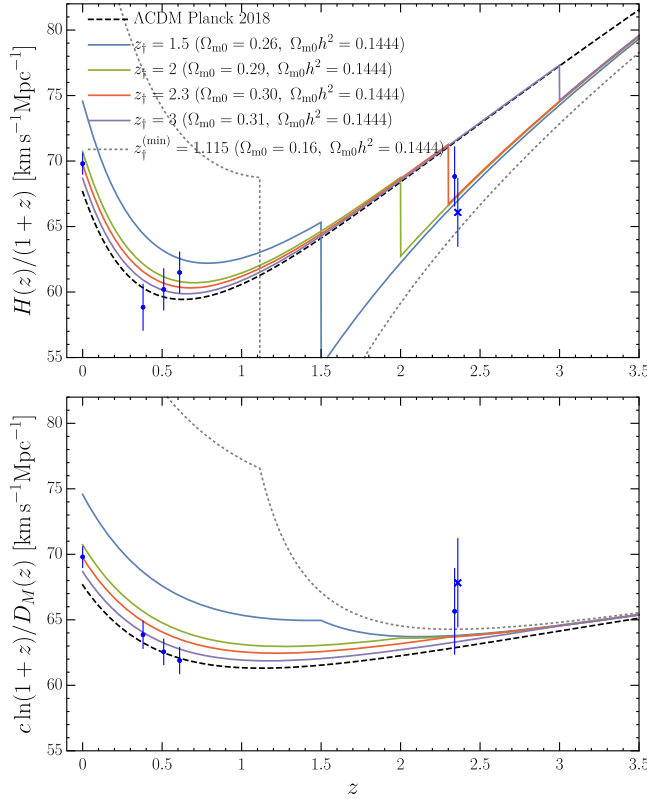


FIG. 2. H_0 versus z_{\dagger} for the Λ_s CDM model (solid curve) and the Λ CDM model (dashed line). The values are calculated by fixing $D_M(z_*)$ and $\rho_m(z_*)$ (and hence ρ_{m0}) to that of Λ CDM using the mean values of the *Planck* 2018 TT, TE, EE + lowE + lensing results [6]. The gray band is the model-independent TRGB measurement $H_0 = 69.8 \pm 0.8 \text{ km s}^{-1} \text{ Mpc}^{-1}$ [77] and the blue band is the Cepheid measurement $H_0 = 74.03 \pm 1.42 \text{ km s}^{-1} \text{ Mpc}^{-1}$ [75].

F2:1
 F2:2
 F2:3
 F2:4
 F2:5
 F2:6
 F2:7
 F2:8

594 increases, H_0 decreases, approaching the value of
 595 Λ CDM as $z_{\dagger} \rightarrow \infty$. This is for two reasons: first, as z_{\dagger}
 596 increases, the portion of the $D_M(z_*)$ integral that is
 597 over negative values of Λ_s decreases and hence requires
 598 less compensation from the positive Λ_s portion including
 599 H_0 ; second, as z_{\dagger} increases, the sign-switching feature of
 600 Λ_s becomes rapidly less effective since, for large z_{\dagger} , matter
 601 is the dominant energy component of the Universe at the
 602 time of the sign switch and the effect of a negative Λ_s
 603 on the evolution of $H(z)$ is negligible. If we consider
 604 $z_{\dagger} = 3$, just before the cosmological constant becomes
 605 negative ($z \rightarrow z_{\dagger}^-$), the matter is already by far the domi-
 606 nant component of the Universe, viz., $\Omega_m(z = 3) \approx 0.96$,
 607 corresponding to only $|\Omega_{\Lambda_s}/\Omega_m| \approx 0.04$. It is intriguing
 608 that, for $z_{\dagger} = 2.3$, which is almost as high as z_{\dagger} can get
 609 without losing the improved agreement with the Ly- α
 610 data, the H_0 value is in excellent agreement with $H_0 =$
 611 $69.8 \pm 0.8 \text{ km s}^{-1} \text{ Mpc}^{-1}$ [77] (revised as $H_0 = 69.6 \pm$
 612 $0.8 \text{ km s}^{-1} \text{ Mpc}^{-1}$ in Ref. [79]) from a recent calibration
 613 of the tip of the red giant branch (TRGB) applied to type Ia
 614 supernovae. Both of these effects on H_0 and $H(z \approx 2.34)$
 615 suggest that Λ_s CDM might be most effective for $z_{\dagger} \lesssim 2.34$.
 616 In line with this, as Fig. 2 demonstrates, H_0 is greater
 617 for smaller values of z_{\dagger} ; for $z_{\dagger} = 1.5$, H_0 goes up to
 618 $\approx 74.5 \text{ km s}^{-1} \text{ Mpc}^{-1}$, so $z_{\dagger} > 1.5$ covers all of the recent



F3:1 FIG. 3. Comoving Hubble parameter and the comoving angular
 F3:2 diameter distance versus redshift for various z_{\dagger} values for the
 F3:3 Λ_s CDM model. All of the plots are drawn by fixing $D_M(z_*)$ and
 F3:4 $\rho_m(z_*)$ (and hence fixing ρ_{m0}) to that of the Λ CDM model using
 F3:5 mean values of the *Planck* 2018 TT, TE, EE + lowE + lensing
 F3:6 Ω results. We consider the observational $H(z)$ values (blue error
 F3:7 bars), $H_0 = 69.8 \pm 0.8 \text{ km s}^{-1} \text{ Mpc}^{-1}$ from the TRGB [77],
 F3:8 consensus Galaxy BAO (from $z_{\text{eff}} = 0.38, 0.51, 0.61$), and
 F3:9 DR14 Ly- α BAO (from $z_{\text{eff}} = 2.34, 2.35$) [84,85,148].

619 local measurements of H_0 , including the largest H_0
 620 estimations by the SH0ES Collaboration (see Refs. [73–
 621 79]). However, looking at the bottom panel of Fig. 3, we see
 622 that as z_{\dagger} gets smaller, a greater tension with the comoving
 623 angular diameter distance measurements from Galaxy BAO
 624 data is generated. In fact, Fig. 3 seems to suggest that the
 625 smaller the value of z_{\dagger} , the greater the tension with the
 626 Galaxy BAO data, and the extent of this effect in limiting the
 627 increase in H_0 is not clear without a robust observa-
 628 tional analysis.

629 Ω The discrepancy of the latest SH0ES H_0 determina-
 630 $H_0^{\text{R20}} = 73.2 \pm 1.3 \text{ km s}^{-1} \text{ Mpc}^{-1}$ [76] and Λ CDM *Planck*
 631 2018 constraint $H_0 = 67.36 \pm 0.54 \text{ km s}^{-1} \text{ Mpc}^{-1}$ [6] is
 632 equivalent to the discrepancy of the Pantheon SNIa absolute
 633 magnitudes, which have a value $M_B^{\text{Planck}} = -19.401 \pm$
 634 0.027 mag [149] when calibrated using the CMB sound
 635 horizon and propagated via BAO measurements to low z
 636 (inverse distance ladder, $z \approx 1100$), which is in significant
 637 tension (3.4σ) with the value $M_B^{\text{R20}} = -19.244 \pm 0.037 \text{ mag}$
 638 [146] (using Pantheon SNIa data set [150]) when the

calibration is done using Cepheid stars at $z < 0.01$. Ω 639
 This tension is reflected in the inferred SNIa absolute 640
 magnitudes from $M_{B,i} = m_{B,i} - \mu(z_i)$ [where $\mu(z_i) =$ 641
 $5 \log_{10} \left[\frac{1+z_i}{10 \text{ pc}} \int_0^{z_i} \frac{cdz}{H(z)} \right]$ is the distance modulus for the spatially 642
 flat RW metric and $m_{B,i}$ is the measured apparent magnitude 643
 of the supernovae at redshift z_i ($z_i > 0.01$)] using the distance 644
 modulus corresponding to the Λ CDM *Planck* 2018 curve in 645
 Fig. 3, which are in tension with M_B^{R20} from Cepheid 646
 calibrators (see black error bars in Fig. 4 and the caption 647
 of the figure for information about the $m_{B,i}$ data that we used). 648
 On the other hand, we see from the figure that for $z_{\dagger} = 2.3$ 649
 (red bars) (i.e., when Λ_s CDM agrees with the TRGB H_0 650
 measurement) the inferred $M_{B,i}$ values are systematically 651
 shifted upwards, relaxing the tension with M_B^{R20} , and for 652
 $z_{\dagger} = 1.5$ (blue bars) (i.e., when Λ_s CDM agrees with the 653
 SH0ES H_0 measurement) the estimated absolute magnitudes 654
 from Λ_s CDM are in excellent agreement with M_B^{R20} . It is no 655
 surprise that Λ_s CDM results in greater $M_{B,i}$ values compared 656
 to Λ CDM for $z < z_{\dagger}$, because it is guaranteed that, compared 657
 to Λ CDM with the same $D_M(z_*)$ and $\Omega_{m0}h^2$ values, Λ_s CDM 658
 has greater $H(z < z_{\dagger})$ values, making its $\mu(z < z_{\dagger})$ smaller. Ω 659
 A subtler point is that, although $H(z > z_{\dagger})$ is smaller for 660
 Λ_s CDM, it will keep resulting in greater $M_{B,i}$ values up to 661
 $z \sim z_*$ since the smaller value of the $\mu(z)$ of Λ_s CDM catches 662
 up to Λ CDM only at the redshift to which their angular 663
 diameter distance is equal, i.e., at last scattering for which 664
 $D_M(z_*)$ is the same among these models. In addition, since 665
 smaller z_{\dagger} values amplify the above-mentioned deviance of 666
 Λ_s CDM, $M_{B,i}$ are inversely correlated with z_{\dagger} just as H_0 is. 667
 An important point is that Λ_s CDM not only systematically 668

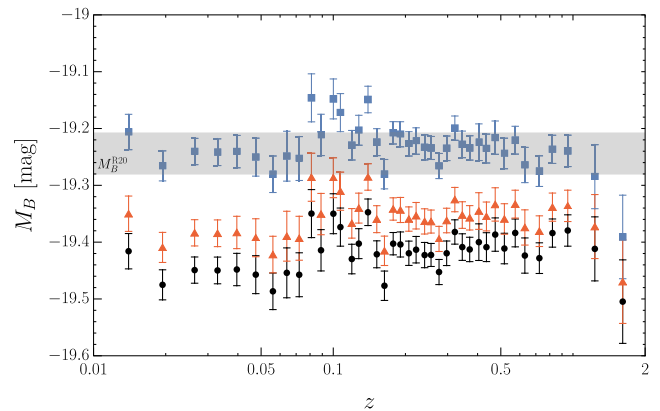


FIG. 4. Inferred SNIa absolute magnitudes $M_{B,i} = m_{B,i} - \mu(z_i)$ 641
 of the binned Pantheon sample containing SNIa apparent magni- 642
 tudes $m_{B,i}$ (with 68% C.L. error bars) [150] for the distance 643
 moduli $\mu(z_i)$ assuming $z_{\dagger} = 1.5$ (blue) (which is in excellent 644
 agreement with the SH0ES H_0 value), $z_{\dagger} = 2.3$ (red) (which is in 645
 excellent agreement with the TRGB H_0 value), and Λ CDM 646
Planck 2018 (black), all calculated using the corresponding $H(z)$ 647
 functions given in Fig. 3 with matching colors. The grey bar is the 648
 68% C.L. constraint from Cepheid calibrations [146]. 649

669 results in higher $M_{B,i}$ values, but also respects the internal
 670 consistency of the SH0ES measurements by simultaneously
 671 matching their H_0 and M_B constraints [73–76,146,147]. This
 672 is not true in general for models with deviations from Λ CDM
 673 at low redshifts, e.g., models with a dynamical DE equation-
 674 of-state parameter, or models of smoothly nonminimally
 675 interacting DE [145,146,151–154]; however, see Ref. [155]
 676 for an analysis in this context excluding CMB data, and
 677 Ref. [156–159] for astrophysical (rather than cosmological)
 678 approaches addressing the M_B tension.

679 As a final remark for this section, we notice that the
 680 condition for an ever-expanding Universe given in Eq. (5)
 681 implies

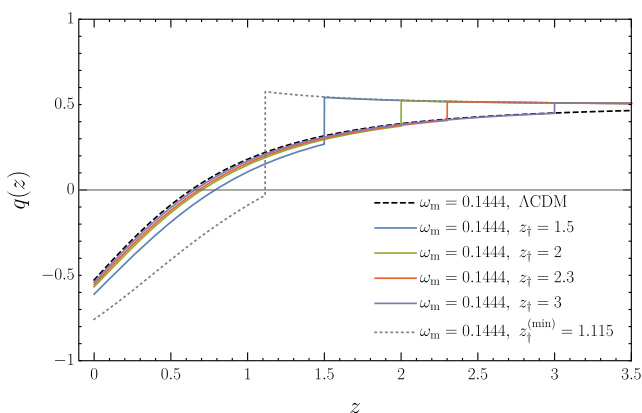
$$z_{\dagger}^{(\min)} = \left(\frac{h_{(\max)}^2}{\omega_m} - 1 \right)^{\frac{1}{3}} - 1, \quad (8)$$

682 where $\omega_m \equiv \Omega_{m0} h^2 \propto \rho_{m0}$ and $h_{(\max)}^2$ is the maximum h
 684 value attainable while satisfying the constraint on $D_M(z_*)$
 685 by the ever-expanding Λ_s CDM Universe for a given ω_m .

686 **15** This also determines $\Omega_m^{(\min)}$, and thereby $\Omega_{\Lambda}^{(\max)}$ as well. We
 687 solve numerically that $z_{\dagger}^{(\min)} \approx 1.1$ for $\omega_m = 0.1444$ (this
 688 value is chosen based on *Planck* 2018 [6], as in Fig. 3); see

689 **16** Fig. 6. We plot the deceleration parameter in Fig. 5 for z_{\dagger}
 690 values, including $z_{\dagger} \approx z_{\dagger}^{(\min)}$ for which the acceleration
 691 starts at z_{\dagger} and not z_c . It is astonishing that even for this
 692 extreme value $z_{\dagger} = 1.115$, which is approximately the limit
 693 of the ever-expanding Universe condition we obtained
 694 while ensuring the consistency with the *Planck* CMB data,
 695 the good representation of the Ly- α data remains, as seen in
 696 Fig. 3. This shows that it is an intrinsic feature of the
 697 Λ_s CDM scenario, which provides an AdS background for
 698 $z > z_{\dagger}$, to be consistent with the available cosmological
 699 data from $z \gtrsim 1$.

700 To summarize, the Λ_s CDM model has the potential to
 701 resolve both the H_0 and M_B tensions while remaining
 702 consistent with the CMB data; the pre-recombination



F5:1 FIG. 5. Evolution of the deceleration parameter $q(z)$ for various
 F5:2 z_{\dagger} values, including $z_{\dagger} \approx z_{\dagger}^{(\min)}$, corresponding to Fig. 3.

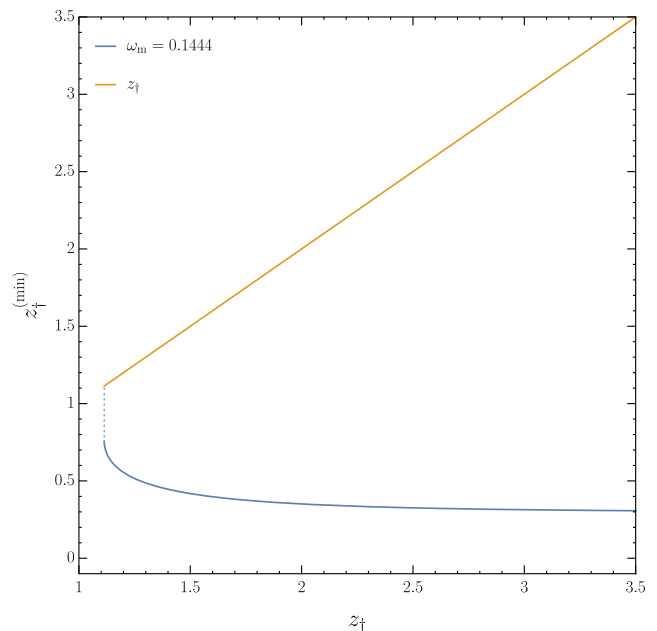


FIG. 6. We solve numerically that $z_{\dagger}^{(\min)} \approx 1.1$. The point equa-
 tion (8) is satisfied, where the straight line (orange) and the curve
 (blue) intersect, is the solution.

703 physics were practically untouched in this analysis. The
 704 model comes with the additional benefit of better agreeing
 705 with the Ly- α measurements for $z_{\dagger} \lesssim 2.34$. However, the
 706 comoving angular diameter distance measurements from
 707 Galaxy BAO oppose the amelioration in H_0 and $M_{B,i}$ by
 708 insisting that z_{\dagger} does not attain very small values.
 709 This opposition may permit a partial alleviation of
 710 the H_0 tension rather than its resolution when, e.g., $H_0 =$
 711 $74.03 \pm 1.42 \text{ km s}^{-1} \text{ Mpc}^{-1}$ from the Cepheid measure-
 712 ment of H_0 [75] is considered; however, it may allow
 713 for a full resolution if one considers $H_0 = 69.8 \pm$
 714 $0.8 \text{ km s}^{-1} \text{ Mpc}^{-1}$ from the TRGB measurement of
 715 H_0 [77], which might prove to be sufficient with forth-
 716 coming observations. There appears to be an interval
 717 $1.5 \lesssim z_{\dagger} \lesssim 2.34$ where the comoving angular diameter
 718 distance data of Galaxy BAO can reconcile with the Ly-
 719 α BAO and H_0 measurements within Λ_s CDM. The
 720 observational analysis in the next section will reveal
 721 how efficient the features of the Λ_s CDM model can work
 722 to alleviate the tensions prevailing in the standard cosmo-
 723 logical model when confronted with data.

III. OBSERVATIONAL CONSTRAINTS AND RESULTS

724 Considering the background and perturbation dynamics,
 725 in what follows we explore the full parameter space of the
 726 Λ_s CDM model and, for comparison, that of the standard
 727 Λ CDM model. The baseline seven free parameters of the
 728 Λ_s CDM model are
 729
 730

$$\mathcal{P} = \{\omega_b, \omega_c, \theta_s, A_s, n_s, \tau_{\text{reio}}, z_{\dagger}\}, \quad (9)$$

732 where the first six parameters are the baseline parameters of
 733 the standard Λ CDM model: $\omega_b = \Omega_b h^2$ and $\omega_c = \Omega_c h^2$ are
 734 the physical density parameters of baryons and cold dark
 735 matter today, respectively, θ_s is the ratio of the sound
 736 horizon to the angular diameter distance at decoupling, A_s
 737 is the power of the primordial curvature perturbations
 738 at $k = 0.05 \text{ Mpc}^{-1}$, n_s is the power-law index of the
 739 scalar spectrum, and τ_{reio} is the Thomson scattering optical
 740 depth due to reionization. We use uniform priors $\omega_b \in$
 741 $[0.018, 0.024]$, $\omega_c \in [0.10, 0.14]$, $100\theta_s \in [1.03, 1.05]$,
 742 $\ln(10^{10} A_s) \in [3.0, 3.18]$, $n_s \in [0.9, 1.1]$, and $\tau_{\text{reio}} \in [0.04,$
 743 **21** $0.125]$ for the common free parameters of model param-
 744 eters and $z_{\dagger} \in [1, 3]$ for the additional free parameter of
 745 Λ_s CDM, which is determined in accordance with the
 746 discussions regarding z_{\dagger} in Sec. II A.

747 In order to constrain the models, we use the latest *Planck*
 748 CMB and BAO data: we use the recently released full
 749 *Planck* (2018) [6] CMB temperature and polarization data
 750 which consist of the low- l temperature and polarization
 751 likelihoods at $l \leq 29$, temperature (TT) at $l \geq 30$, polari-
 752 zation (EE) power spectra, and cross correlation of temper-
 753 ature and polarization (TE). The *Planck* (2018) CMB
 754 lensing power spectrum likelihood [160] is also included.
 755 Along with the *Planck* CMB data, we consider the high-
 756 precision BAO measurements at different redshifts up to
 757 $z = 2.36$, viz., Ly- α DR14, BAO-Galaxy consensus, MGS,
 758 and 6dFGS as presented in Refs. [3,84,85,148,161,162].
 759 It is worth noting that we include Ly- α measurements in our
 760 BAO compilation as they have a substantial impact on the
 761 parameters of Λ_s CDM, whereas they have a minor impact
 762 on the parameters of Λ CDM, which is why they were

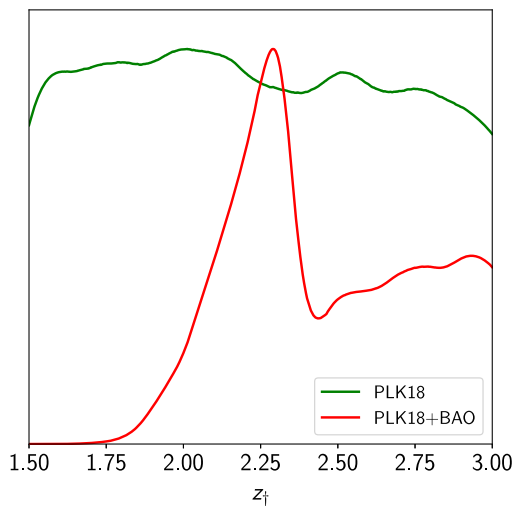
763 excluded from the default BAO compilation by the *Planck*
 764 (2018) Collaboration [6]. We do not include BBN con-
 765 straints on ω_b so that we can compare the constraints on ω_b
 766 predicted from our analysis for different models with those
 767 from BBN without bias. We have implemented the model
 768 in a modified version of the CosmoMC [163] code to
 769 sample over the parameter space and produce posterior
 770 distributions, and used the MCEvidence [164] algorithm
 771 to compute the Bayesian evidence used to perform a
 772 model comparison through the Jeffreys' scale [165]. See
 773 Ref. [166], and references therein, for an extended review
 774 of the cosmological parameter inference and model selec-
 775 tion procedure. We obtain the observational constraints on
 776 all of the parameters of the models— Λ_s CDM, Λ_s CDM +
 777 $z_{\dagger} = 2.32$ (a particular case of Λ_s CDM), and Λ CDM (for
 778 comparison purposes)—by using first only the CMB data
 779 and then the combined CMB + BAO data.

780 Table I displays the constraints at the 68% C.L. on the
 781 free parameters— $10^2 \omega_b$, ω_c , $100\theta_s$, $\ln(10^{10} A_s)$, n_s , τ_{reio} ,
 782 and z_{\dagger} —as well as some derived parameters—the dust
 783 density parameter today Ω_m , the Hubble constant H_0 , the
 784 amplitude of matter fluctuation on $8h^{-1} \text{ Mpc}$ comoving **22**
 785 scale σ_8 , and the combination $S_8 \equiv \sigma_8 \sqrt{\Omega_m/0.3}$ —from
 786 CMB and CMB + BAO data sets separately. We notice
 787 tight constraints on all of the model parameters from the
 788 combined CMB + BAO data, as expected. The additional
 789 parameter z_{\dagger} in Λ_s CDM is not constrained by the CMB
 790 data alone, as may also be seen from Fig. 7 where the one-
 791 dimensional marginalized distributions of z_{\dagger} are shown
 792 from the CMB and CMB + BAO data.

793 In Fig. 7, we see that the one-dimensional marginalized
 794 distribution for z_{\dagger} is quite flat for the CMB-only analysis
 795 (the green curve). The CMB data is insensitive to the value

TABLE I. Constraints (68% C.L.) on the free and some derived parameters of the Λ_s CDM and standard Λ CDM models for CMB and CMB + BAO data. The parameter H_0 is measured in units of $\text{km s}^{-1} \text{ Mpc}^{-1}$. In the last three rows, the best fit ($-2 \ln \mathcal{L}_{\text{max}}$), the log-Bayesian evidence ($\ln \mathcal{Z}$), and the relative log-Bayesian evidence $\Delta \ln \mathcal{Z} = \ln \mathcal{Z}_{\text{reference}} - \ln \mathcal{Z}$ are listed.

| Data set | CMB | | | CMB + BAO | | |
|-----------------------------------|-----------------------|-----------------------|---------------------------------------|-----------------------|-----------------------|---------------------------------------|
| | Λ CDM | Λ_s CDM | Λ_s CDM+ $z_{\dagger} = 2.32$ | Λ CDM | Λ_s CDM | Λ_s CDM+ $z_{\dagger} = 2.32$ |
| $10^2 \omega_b$ | 2.235 ± 0.015 | 2.238 ± 0.015 | 2.238 ± 0.015 | 2.244 ± 0.013 | 2.231 ± 0.014 | 2.230 ± 0.013 |
| ω_c | 0.1201 ± 0.0014 | 0.1197 ± 0.0013 | 0.1199 ± 0.0013 | 0.1189 ± 0.0009 | 0.1208 ± 0.0011 | 0.1209 ± 0.0009 |
| $100\theta_s$ | 1.04090 ± 0.00031 | 1.04093 ± 0.00030 | 1.04091 ± 0.00031 | 1.04102 ± 0.00029 | 1.04081 ± 0.00029 | 1.04080 ± 0.00029 |
| $\ln(10^{10} A_s)$ | 3.044 ± 0.016 | 3.043 ± 0.016 | 3.043 ± 0.016 | 3.045 ± 0.016 | 3.043 ± 0.016 | 3.043 ± 0.016 |
| n_s | 0.9646 ± 0.0043 | 0.9657 ± 0.0044 | 0.9655 ± 0.0044 | 0.9673 ± 0.0037 | 0.9633 ± 0.0039 | 0.9632 ± 0.0036 |
| τ_{reio} | 0.0543 ± 0.0078 | 0.0542 ± 0.0078 | 0.0541 ± 0.0078 | 0.0559 ± 0.0078 | 0.0530 ± 0.0077 | 0.0526 ± 0.0075 |
| z_{\dagger} | ... | unconstrained | [2.32] | ... | 2.44 ± 0.29 | [2.32] |
| Ω_m | 0.3162 ± 0.0084 | 0.2900 ± 0.0160 | 0.2967 ± 0.0086 | 0.3090 ± 0.0059 | 0.3035 ± 0.0062 | 0.3029 ± 0.0060 |
| H_0 | 67.29 ± 0.60 | 70.22 ± 1.78 | 69.42 ± 0.71 | 67.81 ± 0.44 | 68.82 ± 0.55 | 68.91 ± 0.48 |
| σ_8 | 0.8117 ± 0.0076 | 0.8223 ± 0.0098 | 0.8186 ± 0.0074 | 0.8090 ± 0.0073 | 0.8207 ± 0.0080 | 0.8215 ± 0.0071 |
| S_8 | 0.8332 ± 0.0163 | 0.8071 ± 0.0210 | 0.8138 ± 0.0166 | 0.8219 ± 0.0127 | 0.8255 ± 0.0128 | 0.8264 ± 0.0126 |
| $-2 \ln \mathcal{L}_{\text{max}}$ | 1386.52 | 1385.73 | 1386.56 | 1394.32 | 1393.77 | 1393.54 |
| $\ln \mathcal{Z}$ | -1424.19 | -1424.22 | -1423.50 | -1431.46 | -1432.77 | -1431.89 |
| $\Delta \ln \mathcal{Z}$ | 0.69 | 0.72 | 0 | 0 | 1.31 | 0.43 |

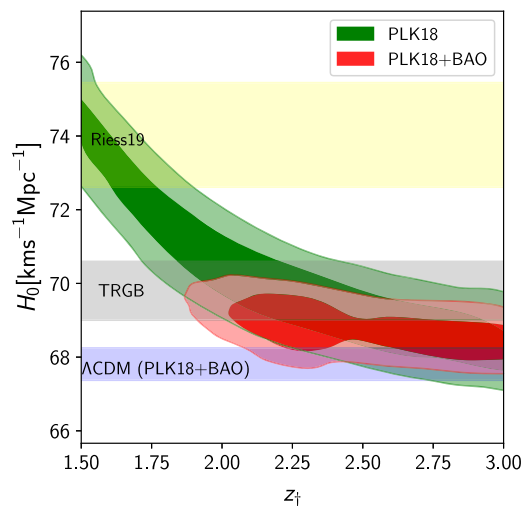


F7:1 FIG. 7. One-dimensional marginalized distributions of the
F7:2 additional free parameter z_+ of the Λ_s CDM model.

796 of z_+ and cannot constrain it, as mentioned in Table I,
797 because for any $z_+ \in [1.5, 3]$ with $\omega_b + \omega_c \sim 0.14$ there
798 exists a Λ_{s0} value for which the comoving angular diameter
799 distance to last scattering fits the CMB measurements.
800 When the BAO data are included in the analysis (the red
801 curve), however, the shape of the distribution changes
802 dramatically, and we see a clear peak at $z_+ \approx 2.3$. This is in
803 line with the discussions in the previous section regarding
804 the Ly- α and Galaxy BAO (SDSS DR14) data. We read off
805 from Fig. 7 that z_+ must be larger than approximately 1.75.
806 The existence of a robust lower bound for z_+ is no surprise,
807 as we anticipated in the previous section from Fig. 3 that
808 smaller z_+ values correspond to higher tension with respect
809 to the Galaxy BAO measurements. This behavior, in turn,
810 decreases the probability of z_+ for values smaller than $z_+ \approx$
811 2.3 just before (in redshift) the redshift of the Ly- α
812 measurements from $z \approx 2.34$. On the other hand, we also
813 see that there is a strong preference for $z_+ \lesssim 2.4$ since for
814 these z_+ values the Λ_s CDM model has substantially better
815 agreement with the Ly- α measurements, which is immedi-
816 ately lost for $z_+ \gtrsim 2.4$; just after (in redshift) the redshift of
817 the Ly- α measurements from $z \approx 2.34$, there is still a
818 plateau-like tail for $z_+ \gtrsim 2.4$ that is reminiscent of the
819 green curve with the addition of a noticeable but insignif-
820 icant trend towards larger z_+ values. We refer readers to
821 Ref. [44] for a similar but more pronounced behavior
822 caused by the Ly- α data (BOSS DR11) in gDE. Once z_+ is
823 restricted to this interval, the fit to the Ly- α data is
824 essentially unaffected by the value of z_+ and the data set
825 is insensitive to z_+ , similar to the CMB-only analysis,
826 except for the slight preference of the larger z_+ values due to
827 the presence of the Galaxy BAO data. In summary, the Ly- α
828 data prefers $z_+ < 2.34$ and the Galaxy BAO data pushes z_+
829 to large values as much as possible; Fig. 7 reflects the
830 competition between the two results in the peak at $z_+ \approx 2.3$.

The asymmetric shape of the posterior for z_+ that is not
831 suitable to be approximated by a Gaussian or another
832 standard distribution renders it not easily interpretable. For
833 this reason, we also study a restriction of the Λ_s CDM
834 model denoted by “ Λ_s CDM + $z_+ = 2.32$ ” for which the
835 only difference compared to Λ_s CDM is that z_+ is fixed to
836 2.32, leaving six free parameters behind as in Λ CDM. The
837 justification for our choice $z_+ = 2.32$ is as follows: in
838 Ref. [44], it was the mean value of the constraints on z_+
839 (denoted by z_* there) both when λ was free and was chosen
840 with a large negative value making the gDE density behave
841 like a step function imitating a sign-switching cosmological
842 constant. Also, $z_+ = 2.32$ is just slightly smaller than the
843 redshift of the Ly- α measurements $z \approx 2.34$, and is sup-
844 posed to provide better agreement with the Ly- α measure-
845 ments; this value is also very close to both the peak and the
846 mean of the red posterior in Fig. 7. The constraints on the
847 Λ_s CDM + $z_+ = 2.32$ model parameters are given in
848 Table I.
849

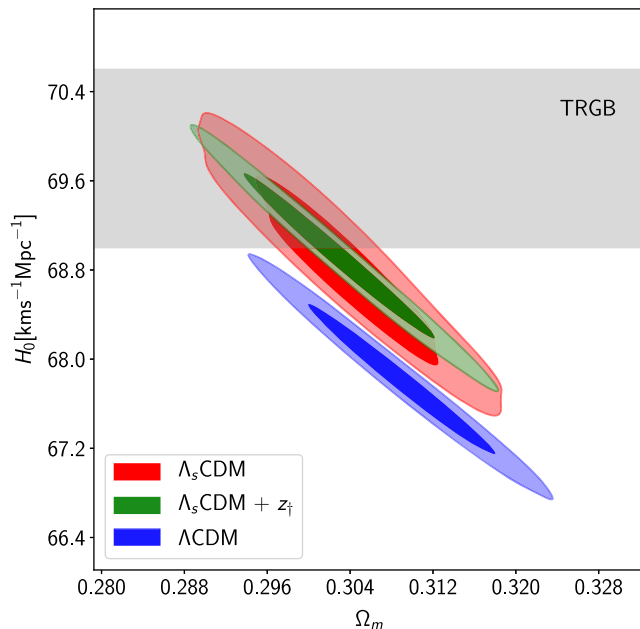
In Fig. 8 we show the two-dimensional (68% and
850 95% C.L.) marginalized distributions of H_0 versus z_+ from
851 the CMB-only data set (green contours) and the combined
852 CMB + BAO data set (red contours). We notice a negative
853 correlation between these two parameters, as expected (see
854 Sec. II A). Since z_+ is not constrained by the CMB-only
855 data set, the green contours scan the whole range of z_+ ; also,
856 as we anticipated from Fig. 2, they encompass even the
857 largest model-independent measurements of H_0 up to
858 $\sim 74 \text{ km s}^{-1} \text{ Mpc}^{-1}$. Due to their strong correlation, the
859 constraints on z_+ are also directly reflected in H_0 , and the
860 exclusion of low z_+ values by the Galaxy BAO data
861 corresponds to the exclusion of the highest H_0 values.
862 For the CMB + BAO data set, $2.15 < z_+ < 2.73$ at
863



F8:1 FIG. 8. Two-dimensional (68% and 95% C.L.) marginalized
F8:2 distributions of H_0 versus z_+ for the Λ_s CDM model, showing a
F8:3 negative correlation between the two parameters, which implies
F8:4 that smaller values of z_+ correspond to larger values of H_0 .

864 68% C.L., as can be read from Table I, and this prevents the
 865 red contours from containing H_0 values as high as the green
 866 one, yet $H_0 = 68.82 \pm 0.55 \text{ km s}^{-1} \text{ Mpc}^{-1}$ ($H_0 = 68.91 \pm$
 867 $0.48 \text{ km s}^{-1} \text{ Mpc}^{-1}$ for the $\Lambda_s\text{CDM} + z_{\dagger} = 2.32$) at
 868 68% C.L., is larger than $H_0 = 67.81 \pm 0.4 \text{ km s}^{-1} \text{ Mpc}^{-1}$
 869 (68% C.L.) of the ΛCDM prediction, and in good agree-
 870 ment with the model-independent TRGB measurement
 871 $H_0 = 69.8 \pm 0.8 \text{ km s}^{-1} \text{ Mpc}^{-1}$ (68% C.L.) [77]. Since
 872 the impact of the sign-switch feature becomes less effective
 873 for larger z_{\dagger} values, both contours approach the ΛCDM
 874 interval of H_0 for large z_{\dagger} , but the error margin is larger for
 875 $\Lambda_s\text{CDM}$ due to the additional errors contributed by the
 876 uncertainty of the extra free parameter z_{\dagger} . Complimentary
 877 to the discussion in this paragraph, in Fig. 9 we show the
 878 two-dimensional (68% and 95% C.L.) marginalized dis-
 879 tributions of H_0 versus Ω_m from CMB + BAO data, which
 880 shows how the H_0 tension is relaxed in $\Lambda_s\text{CDM}$ compared
 881 to ΛCDM . There is a negative correlation between H_0 and
 882 Ω_m for all three models. $\Lambda_s\text{CDM}$ does not overlap with
 883 ΛCDM even at 95% C.L.; this separation is even more
 884 pronounced when the $z_{\dagger} = 2.32$ restriction is considered.
 885 Unsurprisingly, $\Lambda_s\text{CDM} + z_{\dagger} = 2.32$ is contained within
 886 $\Lambda_s\text{CDM}$ and is tightly constrained just like ΛCDM which
 887 has the same number of free parameters.

888 We have discussed in Sec. II A that, within the $\Lambda_s\text{CDM}$
 889 model, the amelioration of the SH0ES H_0 tension is
 890 accompanied by an amelioration of the M_B tension respect-
 891 ing the internal consistency of the SH0ES measurements of



F9:1 FIG. 9. Two-dimensional (68% and 95% C.L.) marginalized
 F9:2 distributions of H_0 versus Ω_m from CMB + BAO data, showing
 F9:3 how the H_0 tension is relaxed in the $\Lambda_s\text{CDM}$ model compared
 F9:4 to the ΛCDM model wherein the horizontal gray band is
 F9:5 for the model = independent TRGB H_0 measurement $H_0 =$
 F9:6 $69.8 \pm 0.8 \text{ km s}^{-1} \text{ Mpc}^{-1}$ [77].

these parameters. We have shown with a preliminary
 analysis that $M_{B,i}$ values calculated by subtracting the
 distance modulus from the apparent magnitudes of the
 binned Pantheon sample [150] should be greater for
 $\Lambda_s\text{CDM}$ compared to the standard model. In this section,
 we do the same $M_{B,i}$ calculations, but now we compute the
 distance modulus values directly from our data analysis;
 indeed, we see in Fig. 10 (the observational counterpart of
 Fig. 4) that the $\Lambda_s\text{CDM}$ models result in $M_{B,i}$ values that
 are systematically higher than those of ΛCDM (as they do
 for H_0 values) and have better agreement with the M_B^{R20}
 value (as they do with local measurements of H_0). For the
 CMB-only analysis in the top panel, the unrestricted
 $\Lambda_s\text{CDM}$, which has the highest H_0 value agreeing the
 best with the SH0ES value, has also the best agreement
 with the M_B^{R20} value among the three models. When BAO is
 included in the data set, the restricted $\Lambda_s\text{CDM}$, compared to
 the other two models, has better agreement with the SH0ES
 H_0 value and thus (as seen in the bottom panel of Fig. 10)
 also with M_B^{R20} . ΛCDM , on the other hand, performs
 substantially worse for both the CMB-only and combined

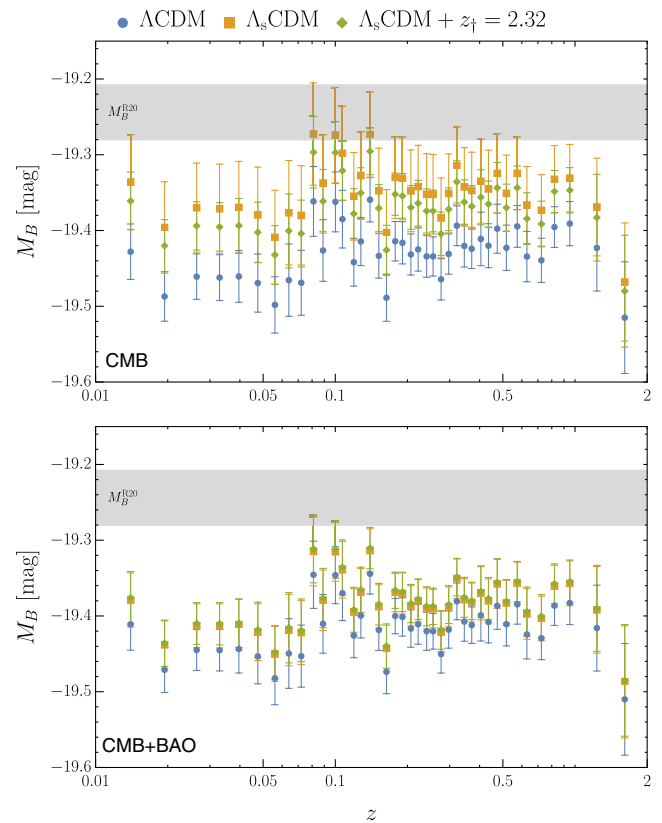


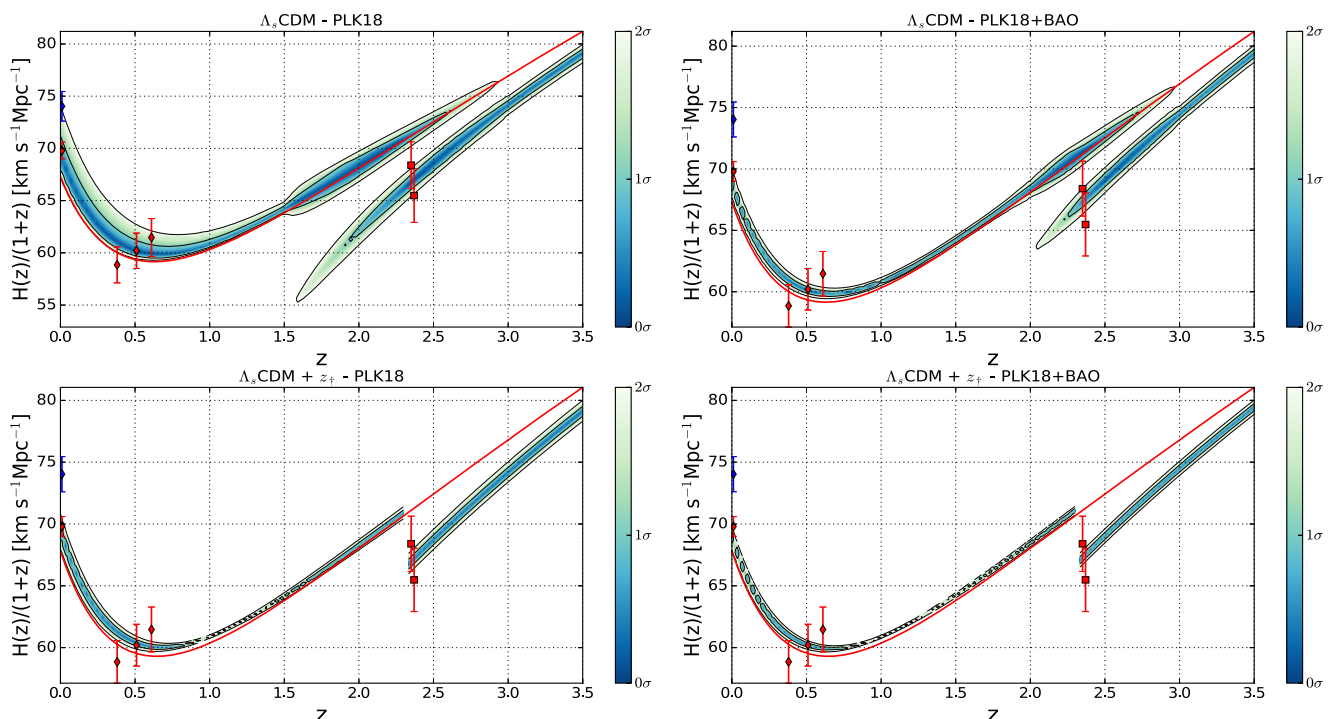
FIG. 10. Observational counterpart of Fig. 4 for the CMB-only
 (top panel) and combined CMB + BAO (bottom panel) analyses.
 The constraints on the absolute magnitudes ($M_{B,i}$) are obtained
 from $M_{B,i} = m_{B,i} - \mu(z_i)$ by using the apparent magnitudes
 ($m_{B,i}$) of the binned Pantheon SNIa sample [150] and the
 constraints we obtained at 68% C.L. on the distance modulus
 values $\mu(z_i)$ for the corresponding SNIa data points.

913 CMB + BAO analyses. As the M_B and SH0ES H_0 tensions
 914 are almost equivalent for Λ_s CDM, just like they are for
 915 Λ CDM, the Galaxy BAO data (which effectively puts an
 916 upper bound on the H_0 values Λ_s CDM can achieve), in
 917 parallel, also puts an upper bound on its $M_{B,i}$ predictions,
 918 limiting the success of the model in alleviating these
 919 tensions.

920 We see that there are certain distinctions between the
 921 CMB and CMB + BAO analyses when parameters related
 922 to matter densities are considered. As seen in Table I, the
 923 CMB-only analysis puts very similar constraints (within
 924 $\sim 1\sigma$ of each other) on ω_b , ω_c , and hence $\omega_m \equiv \omega_b + \omega_c$ for
 925 all three models, while the constraints on Ω_m vary among
 926 the models. In this case, all three ω_b values present similar
 927 discrepancies compared to the BBN constraint $10^2\omega_b =$
 928 2.166 ± 0.019 (namely, $10^2\omega_b = 2.166 \pm 0.015 \pm 0.011$,
 929 where the first error term is due to the uncertainty in the
 930 measurement of the primordial deuterium abundance and the
 931 second error term is due to the uncertainty in the BBN
 932 calculations) [167]. Note that this BBN constraint is based
 933 on the $d(p, \gamma)^3\text{He}$ reaction rate computed in Ref. [168].
 934 Interestingly, including the BAO data in the analysis puts
 935 similar constraints on Ω_m (within $\sim 1\sigma$ of each other) for all
 936 three models while letting ω_b and ω_c vary among the
 937 **26** models. This has some important consequences. First, the
 938 BAO data pull $\omega_m = \Omega_m h^2$ towards smaller values for

Λ CDM while it is pulled towards greater values for both of 939
 the Λ_s CDM models; given the similar Ω_m values for all 940
 three, this results in higher H_0 values for the Λ_s CDM 941
 models compared to Λ CDM. Second, ω_b follows a reverse 942
 trend for all models compared to ω_m , i.e., the BAO data pull 943
 ω_b towards greater values for Λ CDM while it is pulled 944
 towards smaller values for both of the Λ_s CDM models. 945
 Thus, with the inclusion of the BAO data, the discrepancy 946
 with the BBN constraint for ω_b worsens for Λ CDM **27** 947
 while it relaxes for the Λ_s CDM models. We wonder if 948
 this amelioration for the Λ_s CDM model could be 949
 improved if the Galaxy BAO data were not present in the 950
 analysis. Note that in Ref. [167] they also presented the 951
 value $10^2\omega_b = 2.235 \pm 0.037$ (namely, $10^2\omega_b = 2.235 \pm$ 952
 0.016 ± 0.033) when the empirical $d(p, \gamma)^3\text{He}$ reaction rate 953
 in Ref. [169] was used; even in this case, the Λ_s CDM 954
 models are in better agreement with the BBN constraint for 955
 ω_b when the CMB + BAO data set is considered. 956

In Fig. 11 (the observational counterpart of the top panel **28** 957
 of Fig. 3), obtained using the fgivenx PYTHON package 958
 [170], we show $H(z)/(1+z)$ versus z with probability 959
 regions up to 95% C.L. (the darker implies more probable, **29** 960
 as shown in the color bar) in case of CMB (left panel) and 961
 CMB + BAO (right panel) data sets, showing how the 962
 discrepancy with the Ly- α measurements disappears com- 963
 pletely in Λ_s CDM compared to the Λ CDM model, wherein 964

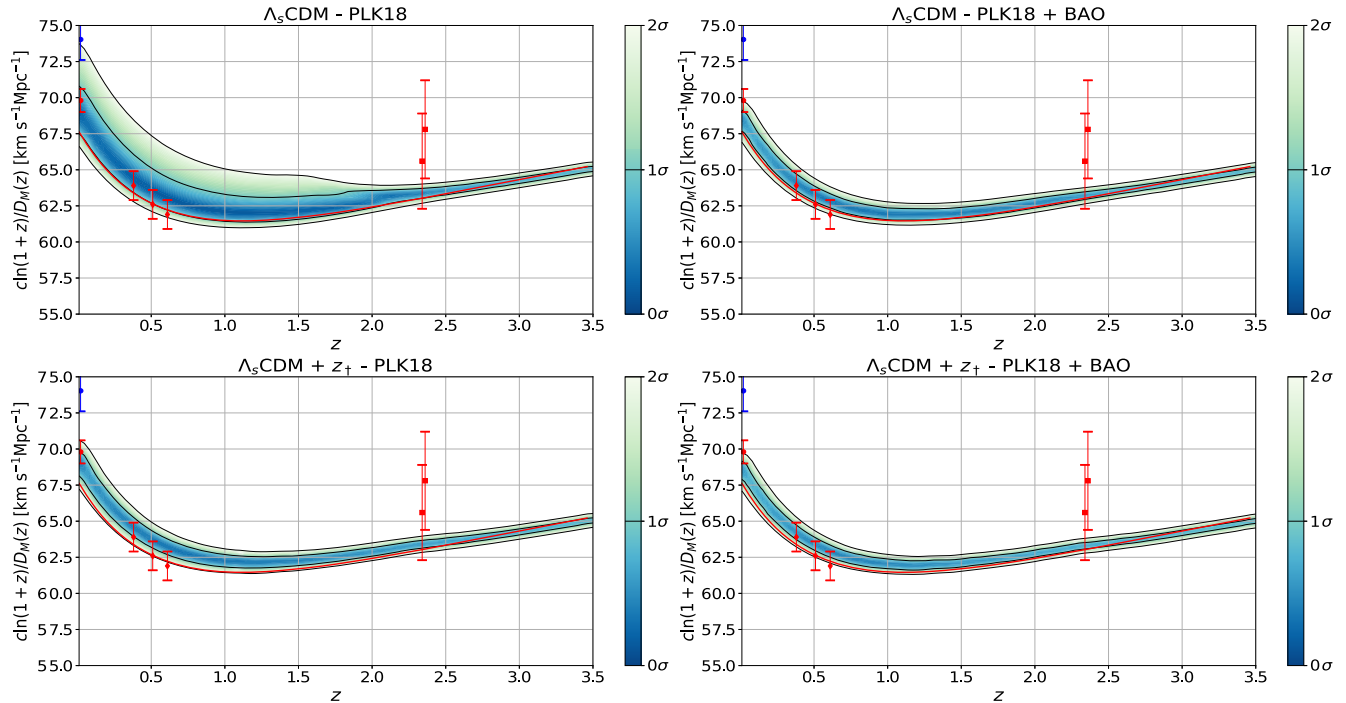


F11:1 FIG. 11. $H(z)/(1+z)$ versus z with 68% and 95% error regions in the case of CMB (left panel) and CMB + BAO (right panel),
 F11:2 showing how the Ly- α data tension is relaxed in the Λ_s CDM model compared to the Λ CDM model, wherein the red curve stands
 F11:3 for the Λ CDM model corresponding to the mean values of the parameters. We show the observational $H(z)$ values (error bars),
 F11:4 $H_0 = 69.8 \pm 0.8 \text{ km s}^{-1} \text{ Mpc}^{-1}$ from the TRGB H_0 [77], $H_0 = 74.03 \pm 1.42 \text{ km s}^{-1} \text{ Mpc}^{-1}$ from the Cepheid measurement H_0 [75],
 F11:5 BAO Galaxy consensus (from $z_{\text{eff}} = 0.38, 0.51, 0.61$), and Ly- α DR14 (from $z_{\text{eff}} = 2.34, 2.35$) [85,148].

965 we show the observational $H(z)$ values $H_0 = 69.8 \pm$
 966 $0.8 \text{ km s}^{-1} \text{ Mpc}^{-1}$ from the TRGB H_0 [77], $H_0 = 74.03 \pm$
 967 $1.42 \text{ km s}^{-1} \text{ Mpc}^{-1}$ from the local measurements using
 968 Cepheid calibrators [75], BAO Galaxy consensus (from
 969 effective redshifts $z_{\text{eff}} = 0.38, 0.51, 0.61$), and Ly- α DR14
 970 (from effective redshifts $z_{\text{eff}} = 2.34, 2.35$) [85,148]. The
 971 inclusion of the BAO data in the analysis substantially
 972 tightens the constraints on $H(z)$ for both models. This also
 973 lowers the maximum H_0 value contained within the 2σ
 974 contours for both models, and this effect is more pro-
 975 nounced in the unrestricted $\Lambda_s\text{CDM}$ due to the truncation
 976 of the smaller z_{\dagger} values by the Galaxy BAO data. Indeed,
 977 while the unrestricted model is in partial agreement with the
 978 H_0 value from the Cepheid measurements for the CMB-
 979 only analysis, for the CMB + BAO data set a significant
 980 tension appears, but the model is still in very good agree-
 981 ment with the H_0 value from the TRGB measurements. For
 982 $z \gtrsim 2.3$, the mean $H(z)$ curve of ΛCDM is below both of
 983 the $\Lambda_s\text{CDM}$ models, and for $z \lesssim 1.5$ it (including H_0) is
 984 even excluded in the 95% C.L. For $z \gtrsim 3$, both $\Lambda_s\text{CDM}$
 985 models strongly exclude the mean $H(z)$ curve of ΛCDM by
 986 preferring lower values, but the unrestricted $\Lambda_s\text{CDM}$ has an
 987 interval of compatibility with ΛCDM for $2.3 \lesssim z \lesssim 3$
 988 **30** at the cost of losing its improved fit to the Ly- α data.
 989 It is not clear from this figure how $\Lambda_s\text{CDM}$, compared
 990 to the ΛCDM model, responds to the Galaxy BAO data; as
 991 we have discussed in the previous sections, the opposition

992 of the Galaxy BAO data to the smaller z_{\dagger} values is based
 993 on the comoving angular diameter distance, $D_M(z)$
 994 measurements.

995 In Fig. 12 (the observational counterpart of the bottom
 996 panel of Fig. 3) we show $\mathcal{D}(z) \equiv c \ln(1+z)/D_M(z)$ versus
 997 z with probability regions up to 95% C.L. for both $\Lambda_s\text{CDM}$
 998 models, and the mean $\mathcal{D}(z)$ curve for the ΛCDM model.
 999 We see from the top left panel that the distribution for the
 1000 unrestricted $\Lambda_s\text{CDM}$ for the CMB-only analysis diffuses to
 1001 substantially higher values compared to ΛCDM , and is
 1002 almost always above ΛCDM ; in fact, the mean curve for
 1003 ΛCDM acts almost as a lower bound for the 2σ contours
 1004 of $\Lambda_s\text{CDM}$. Note that the lowest parts of the contours
 1005 correspond to the highest redshifts for the sign switch,
 1006 i.e., to $z_{\dagger} \sim 3$. This behavior of elevated $\mathcal{D}(z)$ translates into
 1007 the preference for higher H_0 values at $z = 0$ in the presence
 1008 of the sign switch. When the BAO data is included in the
 1009 analysis, the posterior changes very slightly around the Ly-
 1010 α data and the improved agreement is present for both data
 1011 sets; in contrast, the inclusion of the BAO data strictly
 1012 reduces the spread of the distribution at lower z values and
 1013 excludes $H_0 \gtrsim 70 \text{ km s}^{-1} \text{ Mpc}^{-1}$ in the 2σ C.L., but the
 1014 mean curve for ΛCDM still acts almost as a lower bound.
 1015 This shows that higher $\mathcal{D}(z)$ values compared to ΛCDM are
 1016 characteristic of the $\Lambda_s\text{CDM}$ model. For the $\Lambda_s\text{CDM} +$
 1017 $z_{\dagger} = 2.32$ model, the story is very similar but less empha-
 1018 sized. The spread of the posterior is thinner due to the



F12:1 FIG. 12. $c \ln(1+z)/D_M(z) \equiv \mathcal{D}(z)$ versus z with 68% and 95% error regions in the case of CMB (left panel) and CMB + BAO
 F12:2 (right panel) data. We show the observational $H(z)$ values (error bars), $H_0 = 69.8 \pm 0.8 \text{ km s}^{-1} \text{ Mpc}^{-1}$ from the TRGB H_0 [77],
 F12:3 $H_0 = 74.03 \pm 1.42 \text{ km s}^{-1} \text{ Mpc}^{-1}$ from the Cepheid measurement H_0 [75], BAO Galaxy consensus (from $z_{\text{eff}} = 0.38, 0.51, 0.61$), and
 F12:4 Ly- α DR14 (from $z_{\text{eff}} = 2.34, 2.35$) [85,148].

1019 absence of the uncertainty contributed by z_{\dagger} , and including
 1020 the BAO data in the data set does not have substantial
 1021 effects since the constraints from the BAO data on Λ_s CDM
 1022 are mostly due to the exclusion of the smaller z_{\dagger} by the
 1023 Galaxy BAO data, as it was in Fig. 11. Although the Galaxy
 1024 BAO data does not prefer the lowest z_{\dagger} values for which the
 1025 $\mathcal{D}(z)$ plot is substantially elevated, this effect cannot be
 1026 rephrased as “the larger the z_{\dagger} , the better agreement with
 1027 the Galaxy BAO data” as we anticipated in the preliminary
 1028 investigation in the previous section, because it seems from
 1029 Fig. 12 that $\mathcal{D}(z)$ values that are slightly elevated compared
 1030 to Λ CDM would have better agreement with it. Indeed,
 1031 including the BAO data in the analysis slightly elevates the
 1032 plots of the Λ CDM model.

1033 Table I also presents the values for the matter fluctuation
 1034 amplitude parameter, σ_8 . In the CMB-only analysis, the σ_8
 1035 value for the Λ_s CDM model is slightly higher than that of
 1036 the Λ CDM model. Including BAO data in our analysis
 1037 increases the σ_8 value for Λ_s CDM and decreases it for
 1038 Λ CDM, resulting in an increased difference between the
 1039 two models. It is important to include Ω_m in the discussions
 1040 of σ_8 since there is a discordance among various observa-
 1041 tional data in the $\sigma_8 - \Omega_m$ plane within Λ CDM that is
 1042 usually quantified using S_8 . Predictions of S_8 based on the
 1043 CMB alone are in $2 - 3\sigma$ tension with the measurements
 1044 from dynamical low-redshift cosmological probes (weak
 1045 lensing, cluster counts, redshift-space distortion) within the
 1046 Λ CDM model. This is reflected in the CMB-only analysis
 1047 in Table I, in which the value for Λ CDM reads $S_8 =$
 1048 0.8332 ± 0.0163 compared to $S_8 = 0.766^{+0.020}_{-0.014}$ (KiDS-
 1049 **33** 1000 weak lensing) [171]. Note that the measurement
 1050 from the first-year data of HSC SSP [90] for which $S_8 =$
 1051 $0.804^{+0.032}_{-0.029}$ and also KiDS-450+GAMA [89] finding $S_8 =$
 1052 $0.800^{+0.029}_{-0.027}$ remove this discrepancy; nonetheless, recent
 1053 surveys still predict lower values, e.g., $S_8 = 0.776^{+0.017}_{-0.017}$
 1054 (DES weak lensing and galaxy clustering) [172]. Similar to
 1055 the situation with the Ly- α measurements, alleviating the S_8
 1056 **31** discrepancy within the Λ CDM model and its minimal
 1057 extensions tends to exacerbate the H_0 tension [68]; more-
 1058 over, constraints on S_8 based on the Ly- α data are in
 1059 agreement with the weak lensing surveys which probe
 1060 similar late-time redshift scales as the Ly- α measurements
 1061 **32** [88]. So, it is conceivable that the Λ_s CDM model provides
 1062 a remedy for the S_8 discrepancy while retaining the better
 1063 fit to the local measurements of H_0 , as is the case for the
 1064 Ly- α discrepancy. Indeed, Table I presents the S_8 values for
 1065 the Λ_s CDM models which are lower than those for Λ CDM
 1066 in the CMB-only analysis, i.e., $S_8 = 0.8071 \pm 0.0210$
 1067 for the unrestricted and $S_8 = 0.8138 \pm 0.0166$ for the
 1068 restricted model; see also Fig. 13, which shows the 68%
 1069 and 95% C.L. contours in the $S_8 - \Omega_m$ plane (notice that
 1070 Λ CDM barely overlaps with Λ_s CDM and does not overlap
 1071 **34** with Λ_s CDM + $z_{\dagger} = 2.32$ at 68% C.L.). We see from the
 1072 table that, although σ_8 is the smallest for the Λ CDM among

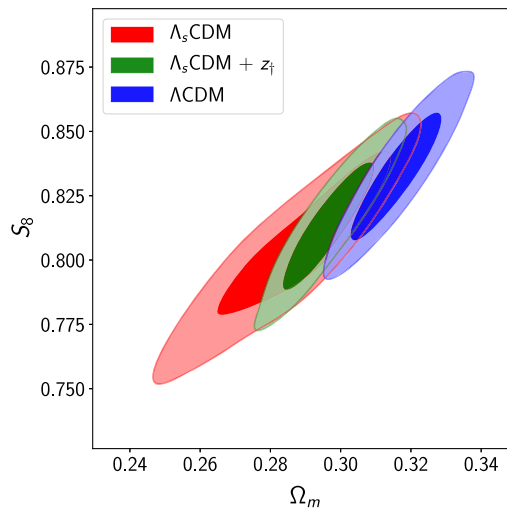


FIG. 13. Two-dimensional (68% and 95% C.L.) marginalized F13:1
 F13:2 distributions of S_8 versus Ω_m from CMB data.

1073 the three models, its Ω_m value greater than 0.3 results in an
 1074 increased S_8 value compared to its σ_8 value; in contrast, the
 1075 Λ_s CDM models have Ω_m values lower than 0.3 which
 1076 result in decreased S_8 values compared to their σ_8 values.
 1077 This results in the lower values of S_8 for Λ_s CDM compared
 1078 to the Λ CDM model. Note that lower z_{\dagger} values correspond
 1079 to lower Ω_m values; this explains why the restricted
 1080 Λ_s CDM model exhibits a higher S_8 value. All three models
 1081 have similar S_8 values when the BAO data is also included
 1082 in the analysis; as before, this is due to the preference for
 1083 higher z_{\dagger} values by the Galaxy BAO data, since Λ_s CDM
 1084 approaches the Λ CDM model for larger z_{\dagger} values and the
 1085 Ω_m values of the extended models are no longer less than
 1086 0.3. Thus, it appears that the Λ_s CDM model partially
 1087 reconciles the CMB data with the low-redshift cosmologi-
 1088 cal probes when S_8 is considered, and could potentially
 1089 resolve the discrepancy in the absence of the Galaxy BAO
 1090 data; however, for a robust conclusion on this matter, the
 1091 constraints on S_8 from low-redshift probes should also be
 1092 investigated within the Λ_s CDM model.

1093 The constraints on the scalar spectral index n_s do not
 1094 differ substantially depending on the data sets and models.
 1095 However, it is worth mentioning that n_s in Λ CDM is
 1096 slightly smaller than the ones in the Λ_s CDM models for the
 1097 CMB-only analysis, while the situation is the opposite for
 1098 the combined CMB + BAO analysis. We notice that, in
 1099 Λ CDM, the inclusion of the BAO data decreases (increases)
 1100 the marginalized value of ω_c ($10^2 \omega_b$) obtained
 1101 in the CMB-only analysis, and this effect is compensated
 1102 by a shift in n_s towards slightly larger values (see Ref. [173]
 1103 for a similar result). Interestingly, it is the other way around
 1104 and relatively more substantial for Λ_s CDM: the inclusion
 1105 of BAO data increases (decreases) the marginalized value
 1106 of ω_c ($10^2 \omega_b$) obtained in the CMB-only analysis, and this
 1107 effect is compensated by a shift in n_s towards smaller
 1108 values.

1109 We found no significant deviations in the constraints on
 1110 the rest of the free parameters in Table I. θ_s is constrained
 1111 robustly and almost the same in all cases, as expected. τ_{reio}
 1112 and $\ln(10^{10}A_s)$ are almost the same for all three models in
 1113 the CMB-only analysis. Including BAO in the analysis
 1114 causes both τ_{reio} and $\ln(10^{10}A_s)$ to go up, resulting in a
 1115 slight decrease in the scaling of subhorizon anisotropies,
 1116 i.e., in $A_s e^{-2\tau_{\text{reio}}}$, for ΛCDM ; in contrast, it causes
 1117 both τ_{reio} and $\ln(10^{10}A_s)$ to go down, resulting in a slight
 1118 increase in the $A_s e^{-2\tau_{\text{reio}}}$ value for the $\Lambda_s\text{CDM}$ models.
 1119 This behavior of τ_{reio} may be explained as follows. The
 1120 reionization optical depth can be calculated using $\tau_{\text{reio}} =$
 1121 $n_{\text{H}}(0)c\sigma_{\text{T}}\int_0^{z_{\text{max}}} dz x_e(z) \frac{(1+z)^2}{H(z)}$ (see, e.g., Ref. [6]), where σ_{T}
 1122 is the Thomson scattering cross section, $n_{\text{H}}(0)$ is the
 1123 present-day total number of hydrogen nuclei, $x_e(z)$ is
 1124 the ratio of the number density at z of the free electrons
 1125 from reionization to the number of total hydrogen nuclei at
 1126 z , and z_{max} is the integration bound that should be chosen
 1127 high enough to allow the entire reionization to be captured
 1128 (i.e., $z_{\text{max}} \geq 50$). Although the shape of $x_e(z)$ is not strictly
 1129 constrained, it is expected to resemble a sigmoid function
 1130 which is approximately zero for $z \geq 10$ and slightly greater
 1131 than unity for $z \leq 6$; it is modeled based on the hyperbolic
 1132 tangent function by the *Planck* Collaboration (2018) [6].
 1133 Assuming $D_M(z_*)$ is the same for all three models in our
 1134 analysis—which is closely related to the above integral—
 1135 we expect lower τ_{reio} values for the $\Lambda_s\text{CDM}$ models as a
 1136 consequence of the suppression of the $z \gtrsim 10$ portion of the
 1137 integral by $x_e(z)$. This is because the $z \gtrsim 10$ portion
 1138 constitutes a lower percentage of the total integral for
 1139 ΛCDM compared to the other two since $H(z > z_{\dagger})$ is
 1140 greater for the ΛCDM model (so its contribution to the
 1141 integral is smaller) in the CMB-only analysis. The results of
 1142 the CMB-only analysis (see Table I) are in line with this
 1143 argument. Following this logic, we expect the inclusion of
 1144 the BAO data in the analysis to slightly increase τ_{reio} for
 1145 $\Lambda_s\text{CDM}$ for two reasons: first, the inclusion of the BAO
 1146 data increases its ω_m value, which implies a greater r_* and
 1147 hence greater $D_M(z_*)$ compared to the CMB-only analysis;
 1148 second, this inclusion results in larger z_{\dagger} values compared
 1149 to the CMB-only analysis, making the model approach
 1150 ΛCDM which we expect to have a higher τ_{reio} value.
 1151 Similar logic based on ω_m (and r_*) may be used to expect a
 1152 higher τ_{reio} value for $\Lambda_s\text{CDM} + z_{\dagger} = 2.32$ and a lower
 1153 value for ΛCDM . Surprisingly, the results in Table I are the
 1154 opposite for all three models. This can be explained by
 1155 changes in $n_{\text{H}}(0)$ and $x_e(z)$ with the inclusion of the BAO
 1156 data, which are powerful enough to win over the effects
 1157 explained above. Indeed, we see that the physical baryon
 1158 density ω_b , which should naturally correlate positively with
 1159 the total number of hydrogen nuclei $n_{\text{H}}(0)$ and hence τ_{reio} ,
 1160 decreases for the $\Lambda_s\text{CDM}$ models and increases for ΛCDM .
 1161 Finally, to quantify which model performs better, we
 1162 compute the Bayesian evidence used to perform a model

comparison through the Jeffreys' scale [174,175]. In 35 163
 Table I, we list the best fit ($-2\ln\mathcal{L}_{\text{max}}$) and (regarding 1164
 the goodness of fit) the log-Bayesian evidence ($\ln\mathcal{Z}$) for 1165
 each of the models along with the Bayes' factor 1166
 ($\Delta\ln\mathcal{Z} = \ln\mathcal{Z}_{\text{reference}} - \ln\mathcal{Z}$)—the log-Bayesian evidence 1167
 for each of the models relative to the reference model, viz., 1168
 the model with the lowest $|\ln\mathcal{Z}|$ value. The interpretation 1169
 of the Bayes' factor according to the Jeffreys' scale is as 1170
 follows: $0 < \Delta\ln\mathcal{Z} \leq 1$ implies that the strength of the 1171
 evidence against the model compared to the reference 1172
 model is weak/inconclusive, while the evidence is definite 1173
 for $1 \leq \Delta\ln\mathcal{Z} < 3$, strong for $3 \leq \Delta\ln\mathcal{Z} < 5$, and very 1174
 strong for $\Delta\ln\mathcal{Z} > 5$ [176]. We see from Table I that all of 1175
 the models fit equally well to the data for both the CMB- 1176
 only and combined CMB + BAO analyses. For the CMB- 1177
 only analysis, the restricted $\Lambda_s\text{CDM}$ model is the reference 1178
 model and there is weak evidence against the other two 1179
 models. In the case of the combined CMB + BAO data 1180
 analysis, ΛCDM is the reference model, and the unre- 1181
 stricted $\Lambda_s\text{CDM}$ model departs from it with definite 1182
 evidence due to the presence of the additional free 1183
 parameter z_{\dagger} . However, we note that $\Lambda_s\text{CDM}$ agrees better 1184
 with the model-independent measurements of H_0 and M_B , 1185
 the constraints on ω_b from BBN, and the constraints on S_8 1186
 from low-redshift probes, which are excluded in the 1187
 observational analyses in the current work. 1188

IV. CONCLUSIONS 1189

In this paper, we first discussed the possibility that 1190
 dark energy models with energy densities that attain 1191
 negative values in the past can alleviate the H_0 tension, 1192
 as well as the discrepancy with the Ly- α BAO measure- 1193
 ments, both of which prevail within the ΛCDM model. The 1194
 so-called graduated dark energy [44], owning this feature, 36 195
 when restricted to its parameter space constrained by 1196
 observations, is phenomenologically well approximated 1197
 by a cosmological constant which switches sign at redshift 1198
 $z \approx 2.32$ to become positive today. It, however, reconciles 37 199
 with the weak energy condition and the bounds on the 1200
 speed of sound at its limit of cosmological constant, which 1201
 comes with a sign-switching feature in contrast to the usual 1202
 cosmological constant (Λ). This led the authors of Ref. [44] 1203
 to conjecture that the Universe transitioned from AdS vacua 1204
 to dS vacua at $z \approx 2.3$. Inspired by this, we have introduced 1205
 the $\Lambda_s\text{CDM}$ model, which promotes the usual cosmological 1206
 constant assumption of the standard ΛCDM model to a 1207
 sign-switching cosmological constant (Λ_s). 1208

The $\Lambda_s\text{CDM}$ model, neglecting radiation, corresponds to 1209
 gluing two Friedmann-Lemaître models at $z = z_{\dagger}$: one with 1210
 a cosmological constant that yields a negative value of 1211
 $\Lambda = -\Lambda_{s0} < 0$, which is superseded by the other with a 1212
 cosmological constant that yields a positive value of 1213
 $\Lambda = \Lambda_{s0} > 0$. The deviation of this model from ΛCDM 1214
 is controlled by its only additional parameter z_{\dagger} , the redshift 1215
 at which the cosmological constant switches sign, for 1216

1217 which the limit $z_{\dagger} \rightarrow \infty$ gives the Λ CDM model. Before
 1218 directly confronting the model with observational data, we
 1219 carried out a preliminary investigation to assess the
 1220 reasonable range of z_{\dagger} , and its effects on the dynamics
 1221 of the Universe. We fixed the physical matter density at the
 1222 CMB last scattering and the comoving angular diameter
 1223 distance to last scattering to those of Λ CDM to ensure good
 1224 consistency with the CMB data. We then found that H_0 is
 1225 inversely correlated with z_{\dagger} , and for $z_{\dagger} = 1.5$ it reaches
 1226 $\approx 74.5 \text{ km s}^{-1} \text{ Mpc}^{-1}$. It is comforting that this value is
 1227 already consistent with even the highest values of model-
 1228 independent local measurements of H_0 by the SHOES
 1229 Collaboration, because the values of z_{\dagger} less than about 1.5
 1230 are strongly disfavored by the Galaxy BAO measurements.
 1231 Next, we showed that, unlike many other models with late-
 1232 time modifications to Λ CDM suggested to address the H_0
 1233 tension, the Λ_s CDM model respects the internal consis-
 1234 tency of the methodology used by the SHOES
 1235 Collaboration to estimate H_0 and M_B (SnIa absolute
 1236 magnitude), and therefore, within the Λ_s CDM model,
 1237 the amelioration of the SHOES H_0 tension should be
 1238 accompanied by an amelioration of the M_B tension.
 1239 Also, it is interesting to observe that, as long as
 1240 $z_{\dagger} \lesssim 2.34$, the model remains in excellent agreement with
 1241 the Ly- α measurements even for $z_{\dagger} \sim 1.1$, which barely
 1242 satisfies the condition that we live in an ever-expanding
 1243 Universe; a good agreement with the Ly- α data is an
 1244 intrinsic feature of the Λ_s CDM model as long as $z_{\dagger} \lesssim 2.34$.
 1245 In light of these discussions, we came to the conclusion that
 1246 the Galaxy and Ly- α BAO measurements would determine
 1247 the lower and upper bounds of z_{\dagger} , respectively. We
 1248 leave the interesting possibility of violating the condition
 1249 $z_{\dagger} \gtrsim 1.1$ to future works. In this case, the Universe passes
 1250 through a contraction phase, which in turn breaks the one-
 1251 to-one correspondence between cosmic time and redshift,
 1252 resulting in signals from the same redshift but two different
 1253 ages of the Universe.

1254 We carried out a robust observational analysis first
 1255 with the full CMB data, and then with the combined CMB +
 1256 BAO data set, to constrain the parameters of the Λ_s CDM
 1257 **38** model, along with its particular case having $z_{\dagger} = 2.32$, and
 1258 the Λ CDM model. We found that the CMB data alone do not
 1259 constrain z_{\dagger} , but the combined CMB + BAO data set
 1260 predicts $z_{\dagger} = 2.44 \pm 0.29$ (68% C.L.) with a peak at
 1261 $z_{\dagger} \approx 2.33$ in the posterior. We found slightly positive
 1262 evidence (Bayesian) in favor of Λ CDM over the Λ_s CDM
 1263 model for the CMB + BAO data set, while all of the models
 1264 **39** fit the data equally well. However, the Λ_s CDM model still
 1265 stands in a privileged position as it removes the discrepancy
 1266 with the Ly- α measurements, has better agreement with the
 1267 BBN constraints on the physical baryon density (ω_b),
 1268 provides a lower S_8 value based on the *Planck* data which
 1269 alleviates its discordance with some low-redshift cosmo-
 1270 logical probes, predicts a higher absolute magnitude M_B
 1271 value for SnIa which is in better agreement with its locally

determined constraints obtained by Cepheid calibrators, and 1272
 also alleviates the H_0 tension, especially when the TRGB H_0 1273
 measurement is considered. Also, it is important to note that 1274
 the amelioration in the last four is not captured by the 1275
 Bayesian evidence as the data/priors on ω_b from BBN, on 1276
 H_0 from local measurements, on S_8 from dynamical 1277
 cosmological probes (weak lensing, cluster counts, red- 1278
 shift-space distortion), and on M_B from its local determi- 1279
 nations obtained by Cepheid calibrators are not included in 1280
 our observational analyses. These improvements come at the **40** 1281
 cost of worsening in describing the comoving angular 1282
 diameter distance measurements from the Galaxy BAO; 1283
 in fact, the preference of larger z_{\dagger} values by the Galaxy BAO 1284
 data prevents the Λ_s CDM model from reaching its full 1285
 potential of having an excellent agreement with even the 1286
 highest local H_0 measurements in consistency with the 1287
 constraints on M_B from Cepheid calibrators, and the lowest 1288
 S_8 measurements. In this regard, when BAO data is 1289
 considered, the Λ CDM model is in conflict with the Ly- α 1290
 measurements, while the Λ_s CDM model is in conflict with 1291
 the Galaxy BAO measurements; forthcoming observations 1292
 will be crucial in determining which model is preferred by 1293
 nature. However, there is an asymmetry between the two 1294
 models in the sense that, if new observations are able to 1295
 remove the conflict of Λ CDM with the Ly- α measurements, 1296
 the discrepancy with the BBN constraints on ω_b , the S_8 1297
 discrepancy, and the unnerving H_0 and M_B tensions remain; 1298
 in contrast, if new observations are able to remove the 1299
 conflict of Λ_s CDM with the Galaxy BAO measurements, it 1300
 can work even better in alleviating the H_0 and M_B tensions 1301
 while retaining its superior agreement with the BBN con- 1302
 straints on ω_b , the Ly- α measurements, and the constraints 1303
 on S_8 from dynamical probes. Confronting the Λ_s CDM 1304
 model by considering BBN and/or M_B priors and additional 1305
 observational data from weak lensing, cluster counts, SnIa, 1306
 cosmic chronometers, etc., along with the CMB and BAO 1307
 data used in this study, would allow a more extensive 1308
 evaluation of the model, and a better assessment of the 1309
 importance of the Galaxy BAO data in conflicting its **41** 1310
 otherwise beneficial phenomena. 1311

The assumptions of the Λ_s CDM model—that the sign 1312
 transition of Λ_s happens instantaneously and that the value 1313
 of Λ_s is exactly the opposite of its present-day value before 1314
 the transition—might be too restrictive both phenomeno- 1315
 logically and (bearing in mind that such phenomena should 1316
 eventually be realized via a mechanism from fundamental 1317
 theories of physics) theoretically. Accordingly, it is possible 1318
 to think of two natural phenomenological extensions to the 1319
 Λ_s CDM model: first, the sign-switching cosmological 1320
 constant described here by a step function can be extended 1321
 via smooth sigmoid functions so that the rapidity of the 1322
 switch can also be controlled; second, one can consider a 1323
 scenario in which the cosmological constant reaches its 1324
 present-day positive value by an arbitrary shift in its value 1325
 rather than a sign switch, and constrain the amount of 1326

1327 change in its value as an extra parameter (in this case,
 1328 additional scenarios with a vanishing or positive-valued
 1329 cosmological constant in the past are also possible, and the
 1330 shift in the cosmological constant need not be positive, but
 1331 obviously a negative shift is not expected considering what
 1332 we have learned from this current study); a third model can
 1333 be constructed by combining these two, which would be
 1334 the most natural one. From the perspective of theoretical
 1335 physics constructions that would underlie the sign switch
 1336 (or the value transition) feature, these extensions will
 1337 be more reasonable and expand the space of possible
 1338 theoretical mechanisms.

1339 One such mechanism can be straightforwardly realized
 1340 in unimodular gravity (UG) [177,178] if the usual vacuum
 1341 energy of QFT suddenly or gradually diffuses to the
 1342 **42** cosmological constant and uplifts its value, say, negative
 1343 in the past, to its present-day observed value. Since the
 1344 usual vacuum energy of QFT does not gravitate in UG, the
 1345 change in its energy density has no effect on the dynamics
 1346 of the Universe, but the change in the value of the
 1347 cosmological constant (which arises naturally as an
 1348 integration constant in UG and contributes to the field
 1349 equations as a geometrical component) does affect the
 1350 dynamics; thus, this mechanism can produce the exact
 1351 phenomenology of Λ_s CDM and all three of its extensions
 1352 depending on the functional form and amount of the
 1353 diffusion. Recently, such a mechanism within UG—for
 1354 which the diffusion, instead of happening from the usual
 1355 vacuum energy of the QFT, happens from the matter
 1356 sector to the cosmological constant—was studied both
 1357 theoretically and phenomenologically to address the H_0
 1358 tension [57,58,179–182]; however, note that this scenario
 1359 is different from Λ_s CDM and its above-mentioned exten-
 1360 sions, as this mechanism uses some energy budget from
 1361 the energy density of the matter sector. The sign switch
 1362 feature of the Λ_s CDM model is reminiscent of the so-
 1363 called Everpresent Λ model [183,184], which was sug-
 1364 gested for addressing the H_0 and L_y - α tensions, in which
 1365 the observed Λ fluctuates between positive and negative
 1366 values with a magnitude comparable to the cosmological
 1367 critical energy density about a vanishing mean, $\langle \Lambda \rangle = 0$,
 1368 in any epoch of the Universe, in accordance with a long-
 1369 standing heuristic prediction of the causal set approach to
 1370 quantum gravity [185]. Nevertheless, the Λ_s CDM model
 1371 suggests that the sign switch of the cosmological constant
 1372 **43** is a single event that happens in the late Universe at $z \sim 2$.
 1373 If we stick to this, namely, a very rapid single transition or
 1374 its limiting case a single instantaneous (discontinuous)
 1375 transition in the value of the cosmological constant, then it
 1376 would be more reasonable to look for a potential origin
 1377 of this phenomenon in a theory of fundamental physics
 1378 by considering it as a first-order phase transition. See
 1379 Ref. [186] for a recent review on well-known cosmic
 1380 phase transitions. Recently, the phase transition approach
 1381 has been used to address the H_0 tension; see, e.g.,

1382 Refs. [50–52], which considered that the DE density 1382
 1383 behaves like the magnetization of the Ising model and 1383
 1384 presented a realization of this behavior within the 1384
 1385 Ginzburg-Landau framework—which is an effective field 1385
 1386 theory (EFT) describing the physics of phase transitions 1386
 1387 without any dependence on the details of relevant micro- 1387
 1388 structures—and Ref. [53], which considered a gravita- 1388
 1389 tional phase transition that is justified from the EFT point 1389
 1390 of view. The model studied in Ref. [50] is phenomeno- 1390
 1391 logically similar but not equivalent to the one-parameter 1391
 1392 extension of Λ_s CDM with an arbitrary shift in the value of 1392
 1393 the cosmological constant, as (in contrast to our approach 1393
 1394 in this work) the cosmological constant is not allowed to 1394
 1395 take negative values (and thereby the model addresses the 1395
 1396 H_0 tension with a shift in the value of the cosmological 1396
 1397 constant at very low redshifts, viz., $z_t = 0.092^{+0.009}_{-0.062}$, signal- 1397
 1398 ing that it could suffer from the M_B tension; see Sec. II A). **44** 1398
 1399 Given the promising advantages of having a negative 1399
 1400 cosmological constant for $z \gtrsim 2$ regarding the cosmological 1400
 1401 tensions, we have discussed throughout this work, and that 1401
 1402 negative cosmological constant is a theoretical sweet spot— 1402
 1403 AdS space/vacuum is welcome due to the AdS/CFT 1403
 1404 correspondence [94] and is preferred by string theory and 1404
 1405 string theory motivated supergravities [95]—, it would be 1405
 1406 most natural to associate this phenomena with a possible 1406
 1407 phase transition from AdS to dS that is derived in string 1407
 1408 theory, string theory motivated supergravities, and theories 1408
 1409 that find motivation from them. The phase transitions from **45** 1409
 1410 AdS to dS (most compatible with our approach and find- 1410
 1411 ings), Minkowski (corresponding to $\Lambda = 0$) to dS, and dS 1411
 1412 to dS pertain to active area of research in theoretical 1412
 1413 physics, but finding four-dimensional dS spacetime solu- 1413
 1414 tions has been a vexing quest and so far the AdS to dS 1414
 1415 transition has rarely been directly linked to physical cosmology 1415
 1416 and particularly dark energy in the literature, see, e.g., 1416
 1417 Ref. [11,103,187–217]. 1417

1418 Finally, both of the above-mentioned extensions of 1418
 1419 Λ_s CDM introduce two extra free parameters on top of 1419
 1420 Λ CDM, and their combination introduces three. Despite **46** 1420
 1421 their excess number of free parameters, which are subject 1421
 1422 to observational constraints, both the promising features 1422
 1423 of the Λ_s CDM model, and the fact that these phenom- 1423
 1424 enological models could act as a guide and a cosmological 1424
 1425 testing ground for the fundamental physics theories giving 1425
 1426 rise to their phenomena, suggest that these extensions are 1426
 1427 worth further studying. Regarding the rapidity of the AdS- 1427
 1428 to-dS transition in a string theory setup, note the com- 1428
 1429 ments against continuous variation of the cosmological 1429
 1430 constant, which could necessitate an instantaneous tran- 1430
 1431 sition as in Λ_s CDM [193]. In this sense, a two-parameter 1431
 1432 extension of Λ CDM with an instantaneous arbitrary shift 1432
 1433 in the value of the cosmological constant could be the 1433
 1434 most natural next phenomenological step of our work 1434
 1435 presented in this paper. 1435

ACKNOWLEDGMENTS

1436
 1437 **47** The authors are grateful to the referee for valuable
 1438 comments and suggestions. The authors thank Mehmet
 1439 Özkan for discussions. Ö. A. acknowledges the support
 1440 **48** by the Turkish Academy of Sciences in scheme of the
 1441 Outstanding Young Scientist Award (TÜBA-GEBİP).

E. Ö. acknowledges the support by The Scientific and 1442
 Technological Research Council of Turkey (TÜBİTAK) **49** 1443
 in scheme of 2211/A National PhD Scholarship Program. 1444
 J. A. V. acknowledges the support provided by FOSEC 1445
 SEP-CONACYT Investigación Básica A1-S-21925, 1446
 FORDECYT-PRONACES-CONACYT/304001/2020, and **50** 1447
 UNAM-DGAPA-PAPIIT IA104221. **51** 1448

1449

- 1450 **52** [1] E. Di Valentino, L. A. Anchordoqui, O. Akarsu, Y. Ali- 1495
 1451 Haimoud, L. Amendola *et al.*, Cosmology intertwined I: 1496
 1452 Perspectives for the next decade, *Astropart. Phys.* **131**, 1497
 1453 **53** 102606 (2021). 1498
 1454 [2] A. G. Riess *et al.* (Supernova Search Team), Observational 1499
 1455 evidence from supernovae for an accelerating Universe and 1500
 1456 a cosmological constant, *Astron. J.* **116**, 1009 (1998). 1501
 1457 [3] S. Alam *et al.* (BOSS Collaboration), The clustering of 1502
 1458 galaxies in the completed SDSS-III baryon oscillation 1503
 1459 spectroscopic survey: Cosmological analysis of the DR12 1504
 1460 galaxy sample, *Mon. Not. R. Astron. Soc.* **470**, 2617 (2017). 1505
 1461 [4] T. M. C. Abbott *et al.* (DES Collaboration), Dark energy 1506
 1462 survey year 1 results: Cosmological constraints from 1507
 1463 galaxy clustering and weak lensing, *Phys. Rev. D* **98**, 1508
 1464 043526 (2018). 1509
 1465 [5] P. A. R. Ade *et al.* (Planck Collaboration), *Planck* 2015 1510
 1466 results. XIII. Cosmological parameters, *Astron. Astrophys.* **594**, A13 (2016). 1511
 1467 **54** [6] N. Aghanim *et al.* (Planck Collaboration), *Planck* 2018 1512
 1468 results. VI. Cosmological parameters, *Astron. Astrophys.* 1513
 1469 **641**, A6 (2020). 1514
 1470 [7] G. Obied, H. Ooguri, L. Spodyneiko, and C. Vafa, De 1515
 1471 Sitter space and the swampland, [arXiv:1806.08362](https://arxiv.org/abs/1806.08362). 1516
 1472 [8] P. Agrawal, G. Obied, P. J. Steinhardt, and C. Vafa, On the 1517
 1473 cosmological implications of the string swampland, *Phys.* 1518
 1474 *Lett. B* **784**, 271 (2018). 1519
 1475 [9] E. Ó Colgáin, M. H. P. M. van Putten, and H. Yavartanoo, 1520
 1476 de Sitter swampland, H_0 tension & observation, *Phys. Lett.* 1521
 1477 *B* **793**, 126 (2019). 1522
 1478 [10] L. Heisenberg, M. Bartelmann, R. Brandenberger, and A. 1523
 1479 Refregier, Dark energy in the swampland, *Phys. Rev. D* **98**, 1524
 1480 123502 (2018). 1525
 1481 [11] M. Cicoli, S. De Alwis, A. Maharana, F. Muia, and F. 1526
 1482 Quevedo, De Sitter vs quintessence in string theory, 1527
 1483 *Fortschr. Phys.* **67**, 1800079 (2019). 1528
 1484 [12] Y. Akrami, R. Kallosh, A. Linde, and V. Vardanyan, The 1529
 1485 landscape, the swampland and the era of precision cos- 1530
 1486 mology, *Fortschr. Phys.* **67**, 1800075 (2019). 1531
 1487 [13] M. Raveri, W. Hu, and S. Sethi, Swampland conjectures 1532
 1488 and late-time cosmology, *Phys. Rev. D* **99**, 083518 (2019). 1533
 1489 [14] E. Ó. Colgáin and H. Yavartanoo, Testing the swampland: 1534
 1490 H_0 tension, *Phys. Lett. B* **797**, 134907 (2019). 1535
 1491 [15] David Tamayo and J. A. Vazquez, Fourier-series expansion 1536
 1492 of the dark-energy equation of state, *Mon. Not. R. Astron.* 1537
 1493 *Soc.* **487**, 729 (2019). 1538
 1494 [16] É. Aubourg *et al.*, Cosmological implications of baryon 1539
 acoustic oscillation measurements, *Phys. Rev. D* **92**, 1540
 123516 (2015). 1541
 [17] W. L. Freedman, Cosmology at a crossroads, *Nat. Astron.* 1542
1, 0121 (2017). 1543
 [18] J. S. Bullock and M. Boylan-Kolchin, Small-scale chal- 1544
 lenges to the Λ CDM paradigm, *Annu. Rev. Astron. As-* 1545
trophys. **55**, 343 (2017). 1546
 [19] E. Di Valentino, Crack in the cosmological paradigm, *Nat.* 1547
Astron. **1**, 569 (2017). 1548
 [20] M. Raveri and W. Hu, Concordance and discordance in 1549
 cosmology, *Phys. Rev. D* **99**, 043506 (2019). 1550
 [21] L. Verde, T. Treu, and A. G. Riess, Tensions between the 1551
 early and the late Universe, *Nat. Astron.* **3**, 891 (2019). 1552
 [22] W. Handley, Curvature tension: Evidence for a closed 1553
 Universe, *Phys. Rev. D* **103**, L041301 (2021). 1554
 [23] E. Di Valentino, A. Melchiorri, and J. Silk, *Planck* **54** 1555
 evidence for a closed Universe and a possible crisis for 1556
 cosmology, *Nat. Astron.* **4**, 196 (2020). 1557
 [24] E. Di Valentino, A. Melchiorri, and J. Silk, Investigating 1558
 cosmic discordance, *Astrophys. J. Lett.* **908**, L9 (2021). 1559
 [25] S. Vagnozzi, E. Di Valentino, S. Gariazzo, A. Melchiorri, 1560
 O. Mena, and J. Silk, The galaxy power spectrum take on 1561
 spatial curvature and cosmic concordance, *Phys. Dark* 1562
Universe **33**, 100851 (2021). 1563
 [26] G. Efstathiou and S. Gratton, The evidence for a spatially 1564
 flat Universe, *Mon. Not. R. Astron. Soc.* **496**, L91 (2020). 1565
 [27] S. Vagnozzi, A. Loeb, and M. Moresco, Eppur è piatto? 1566
 The cosmic chronometers take on spatial curvature and 1567
 cosmic concordance, *Astrophys. J.* **908**, 84 (2021). 1568
 [28] G. Acquaviva, Akarsu, N. Katurci, and J. Alberto Vazquez, 1569
 Simple-graduated dark energy and spatial curvature, *Phys.* 1570
Rev. D **104**, 023505 (2021). 1571
 [29] S. Hee, J. A. Vazquez, W. J. Handley, M. P. Hobson, and 1572
 A. N. Lasenby, Constraining the dark energy equation of 1573
 state using Bayes theorem and the Kullback- 1574
 Leibler divergence, *Mon. Not. R. Astron. Soc.* **466**, 369 1575
 (2017). 1576
 [30] G. B. Zhao *et al.*, Dynamical dark energy in light of the 1577
 latest observations, *Nature (London)* **1**, 627 (2017). 1578
 [31] S. Vagnozzi, New physics in light of the H_0 tension: An 1579
 alternative view, *Phys. Rev. D* **102**, 023518 (2020). 1580
 [32] J. A. Vázquez, D. Tamayo, A. A. Sen, and I. Quiros, 1581
 Bayesian model selection on scalar e -field dark energy, 1582
Phys. Rev. D **103**, 043506 (2021). 1583

- 1540 [33] S. Vagnozzi, S. Dhawan, M. Gerbino, K. Freese, A.
1541 Goobar, and O. Mena, Constraints on the sum of the
1542 neutrino masses in dynamical dark energy models with
1543 $w(z) \geq -1$ are tighter than those obtained in Λ CDM, *Phys.*
1544 *Rev. D* **98**, 083501 (2018).
- 1545 [34] E. Di Valentino, R. Z. Ferreira, L. Visinelli, and U.
1546 Danielsson, Late time transitions in the quintessence field
1547 and the H_0 tension, *Phys. Dark Universe* **26**, 100385
1548 (2019).
- 1549 [35] E. Di Valentino, A. Melchiorri, and J. Silk, Cosmological
1550 constraints in extended parameter space from the Planck
1551 2018 Legacy release, *J. Cosmol. Astropart. Phys.* **01**
1552 (2020) 013.
- 1553 [36] A. Banerjee, H. Cai, L. Heisenberg, E. Ó. Colgáin, M. M.
1554 Sheikh-Jabbari, and T. Yang, Hubble sinks in the low-
1555 redshift swampland, *Phys. Rev. D* **103**, L081305 (2021).
- 1556 [37] T. Delubac *et al.* (BOSS Collaboration), Baryon acoustic
1557 oscillations in the Ly α forest of BOSS DR11 quasars,
1558 *Astron. Astrophys.* **574**, A59 (2015).
- 1559 [38] V. Sahni, A. Shafieloo, and A. A. Starobinsky, Model
1560 independent evidence for dark energy evolution from
1561 baryon acoustic oscillations, *Astrophys. J.* **793**, L40
1562 (2014).
- 1563 [39] E. Di Valentino, E. V. Linder, and A. Melchiorri, Vacuum
1564 phase transition solves the H_0 tension, *Phys. Rev. D* **97**,
1565 043528 (2018).
- 1566 [40] E. Mörtsell and S. Dhawan, Does the Hubble constant
1567 tension call for new physics?, *J. Cosmol. Astropart. Phys.*
1568 **09** (2018) 025.
- 1569 [41] V. Poulin, K. K. Boddy, S. Bird, and M. Kamionkowski,
1570 Implications of an extended dark energy cosmology with
1571 massive neutrinos for cosmological tensions, *Phys. Rev. D*
1572 **97**, 123504 (2018).
- 1573 [42] Y. Wang, L. Pogosian, G. B. Zhao, and A. Zucca, Evo-
1574 lution of dark energy reconstructed from the latest obser-
1575 vations, *Astrophys. J.* **869**, L8 (2018).
- 1576 [43] K. Dutta, Ruchika, A. Roy, A. A. Sen, and M. M. Sheikh-
1577 Jabbari, Beyond Λ CDM with low and high redshift data:
1578 Implications for dark energy, *Gen. Relativ. Gravit.* **52**, 15
1579 (2020).
- 1580 [44] Ö. Akarsu, J. D. Barrow, L. A. Escamilla, and J. A.
1581 Vazquez, Graduated dark energy: Observational hints of
1582 a spontaneous sign switch in the cosmological constant,
1583 *Phys. Rev. D* **101**, 063528 (2020).
- 1584 [45] R. Calderón, R. Gannouji, B. L’Huillier, and D. Polarski,
1585 Negative cosmological constant in the dark sector?, *Phys.*
1586 *Rev. D* **103**, 023526 (2021).
- 1587 [46] A. Bonilla, S. Kumar, and R. C. Nunes, Measurements of
1588 H_0 and reconstruction of the dark energy properties from a
1589 model-independent joint analysis, *Eur. Phys. J. C* **81**, 127
1590 (2021).
- 1591 [47] F. X. Linares Cedeño, N. Roy, and L. A. Ureña-López,
1592 Tracker phantom field and a cosmological constant:
1593 Dynamics of a composite dark energy model.
- 1594 [48] J. A. Vazquez, S. Hee, M. P. Hobson, A. N. Lasenby, M.
1595 Ibison, and M. Bridges, Observational constraints on
1596 conformal time symmetry, missing matter and double dark
1597 energy, *J. Cosmol. Astropart. Phys.* **07** (2018) 062.
- 1598 [49] S. Capozziello, Ruchika, and A. A. Sen, Model-
1599 independent constraints on dark energy evolution from
low-redshift observations, *Mon. Not. R. Astron. Soc.* **484**,
4484 (2019).
- [50] A. Banihashemi, N. Khosravi, and A. H. Shirazi, Phase
transition in the dark sector as a proposal to lessen
cosmological tensions, *Phys. Rev. D* **101**, 123521 (2020).
- [51] A. Banihashemi, N. Khosravi, and A. H. Shirazi,
Ginzburg-Landau theory of dark energy: A framework
to study both temporal and spatial cosmological tensions
simultaneously, *Phys. Rev. D* **99**, 083509 (2019).
- [52] A. Banihashemi, N. Khosravi, and A. Shafieloo, Dark
energy as a critical phenomenon: A hint from Hubble
tension, *J. Cosmol. Astropart. Phys.* **06** (2021) 003.
- [53] M. Farhang and N. Khosravi, Phenomenological gravita-
tional phase transition: Reconciliation between the late and
early Universe, *Phys. Rev. D* **103**, 083523 (2021).
- [54] L. Visinelli, S. Vagnozzi, and U. Danielsson, Revisiting a
negative cosmological constant from low-redshift data,
Symmetry **11**, 1035 (2019).
- [55] G. Ye and Y. Piao, Is the Hubble tension a hint of AdS
around recombination?, *Phys. Rev. D* **101**, 083507 (2020).
- [56] G. Ye and Y. S. Piao, T_0 censorship of early dark energy
and AdS vacua, *Phys. Rev. D* **102**, 083523 (2020).
- [57] A. Perez, D. Sudarsky, and E. Wilson-Ewing, Resolving
the H_0 tension with diffusion, *Gen. Relativ. Gravit.* **53**, 7
(2021).
- [58] F. X. Linares Cedeño and U. Nucamendi, Revisiting
cosmological diffusion models in unimodular gravity
and the H_0 tension, *Phys. Dark Universe* **32**, 100807
(2021).
- [59] Ö. Akarsu, N. Katırcı, S. Kumar, R. C. Nunes, B. Öztürk,
and S. Sharma, Rastall gravity extension of the standard
 Λ CDM model: Theoretical features and observational
constraints, *Eur. Phys. J. C* **80**, 1050 (2020).
- [60] A. Paliathanasis and G. Leon, Dynamics of a two scalar
field cosmological model with phantom terms, *Classical*
Quantum Gravity **38**, 075013 (2021).
- [61] Z. Zhou, G. Liu, and L. Xu, Can late dark energy restore
the Cosmic concordance?, [arXiv:2105.04258](https://arxiv.org/abs/2105.04258).
- [62] S. A. Adil, M. R. Gangopadhyay, M. Sami, and M. K.
Sharma, Late time acceleration due to generic modification
of gravity and Hubble tension, [arXiv:2106.03093](https://arxiv.org/abs/2106.03093).
- [63] A. De Felice, C. Q. Geng, M. C. Pookkillath, and L. Yin,
Reducing the H_0 tension with generalized Proca theory,
J. Cosmol. Astropart. Phys. **08** (2020) 038.
- [64] S. Kumar, R. C. Nunes, and S. K. Yadav, Dark sector
interaction: A remedy of the tensions between CMB and
LSS data, *Eur. Phys. J. C* **79**, 576 (2019).
- [65] S. Kumar, Remedy of some cosmological tensions via
effective phantom-like behavior of interacting vacuum
energy, *Phys. Dark Universe* **33**, 100862 (2021).
- [66] J. C. N. de Araujo, A. De Felice, S. Kumar, and R. C.
Nunes, Minimal theory of massive gravity in the light of
CMB data and the S_8 tension, [arXiv:2106.09595](https://arxiv.org/abs/2106.09595).
- [67] E. Di Valentino, L. A. Anchordoqui, O. Akarsu, Y. Ali-
Haimoud, L. Amendola *et al.*, Cosmology intertwined II:
The Hubble constant tension, *Astropart. Phys.* **131**,
102605 (2021).
- [68] E. Di Valentino, L. A. Anchordoqui, O. Akarsu, Y. Ali-
Haimoud, L. Amendola *et al.*, Cosmology intertwined III:
 $f\sigma_8$ and S_8 , *Astropart. Phys.* **131**, 102604 (2021).

- 1660 [69] E. Di Valentino, L. A. Anchordoqui, O. Akarsu, Y. Ali-
1661 Haimoud, L. Amendola *et al.*, Cosmology intertwined IV:
1662 The age of the Universe and its curvature, *Astropart. Phys.*
1663 **131**, 102607 (2021).
- 1664 [70] L. Perivolaropoulos and F. Skara, Challenges for Λ CDM:
1665 An update, [arXiv:2105.05208](https://arxiv.org/abs/2105.05208).
- 1666 [71] S. Weinberg, The cosmological constant problem, *Rev.*
1667 *Mod. Phys.* **61**, 1 (1989).
- 1668 [72] P. J. E. Peebles and B. Ratra, The cosmological constant
1669 and dark energy, *Rev. Mod. Phys.* **75**, 559 (2003).
- 1670 [73] A. G. Riess *et al.*, A 2.4% determination of the local value
1671 of the Hubble constant, *Astrophys. J.* **826**, 56 (2016).
- 1672 [74] A. G. Riess *et al.*, Milky Way cepheid standards for
1673 measuring cosmic distances and application to gaia
1674 DR2: Implications for the Hubble constant, *Astrophys.*
1675 *J.* **861**, 126 (2018).
- 1676 [75] A. G. Riess, S. Casertano, W. Yuan, L. M. Macri, and D.
1677 Scolnic, Large magellanic cloud cepheid standards provide
1678 a 1% foundation for the determination of the Hubble
1679 constant and stronger evidence for physics beyond Λ CDM,
1680 *Astrophys. J.* **876**, 85 (2019).
- 1681 [76] A. G. Riess, S. Casertano, W. Yuan, J. B. Bowers, L.
1682 Macri, J. C. Zinn, and D. Scolnic, Cosmic distances
1683 calibrated to 1% precision with gaia EDR3 parallaxes
1684 and Hubble space telescope photometry of 75 Milky Way
1685 cepheids confirm tension with Λ CDM, *Astrophys. J. Lett.*
1686 **908**, L6 (2021).
- 1687 [77] W. L. Freedman *et al.*, The Carnegie-Chicago Hubble
1688 program. VIII. An independent determination of the
1689 Hubble constant based on the tip of the red giant branch,
1690 *Astrophys. J.* **882**, 34 (2019).
- 1691 [78] W. Yuan, A. G. Riess, L. M. Macri, S. Casertano, and D.
1692 Scolnic, Consistent calibration of the tip of the red giant
1693 branch in the large magellanic cloud on the Hubble space
1694 telescope photometric system and a re-determination of the
1695 Hubble constant, *Astrophys. J.* **886**, 61 (2019).
- 1696 [79] W. L. Freedman, B. F. Madore, T. Hoyt, I. S. Jang, R.
1697 Beaton, M. Gyoon Lee, A. Monson, J. Neeley, and J. Rich,
1698 Calibration of the tip of the red giant branch (TRGB),
1699 *Astrophys. J.* **891**, 57 (2020).
- 1700 [80] E. Di Valentino, O. Mena, S. Pan, L. Visinelli, W. Yang, A.
1701 Melchiorri, D. F. Mota, A. G. Riess, and J. Silk, In the
1702 realm of the Hubble tension—a review of solutions,
1703 *Classical Quantum Gravity* **38**, 153001 (2021).
- 1704 [81] S. Dodelson and F. Schmidt, *Modern Cosmology*, 2nd ed.
1705 (Academic Press, Elsevier Science, New York, 2021).
- 1706 [82] L. Knox and M. Millea, Hubble constant hunter’s guide,
1707 *Phys. Rev. D* **101**, 043533 (2020).
- 1708 [83] V. Poulin, T. L. Smith, T. Karwal, and M. Kamionkowski,
1709 Early Dark Energy can Resolve the Hubble Tension, *Phys.*
1710 *Rev. Lett.* **122**, 221301 (2019).
- 1711 [84] V. de Sainte Agathe *et al.*, Baryon acoustic oscillations at
1712 $z = 2.34$ from the correlations of Ly α absorption in
1713 eBOSS DR14, *Astron. Astrophys.* **629**, A85 (2019).
- 1714 [85] M. Blomqvist *et al.*, Baryon acoustic oscillations from the
1715 cross-correlation of Ly α absorption and quasars in eBOSS
1716 DR14, *Astron. Astrophys.* **629**, A86 (2019).
- 1717 [86] S. Alam *et al.* (eBOSS Collaboration), Completed SDSS-IV
1718 extended baryon oscillation spectroscopic survey:
1719 Cosmological implications from two decades of spectro-
scopic surveys at the apache point observatory, *Phys. Rev. D*
103, 083533 (2021).
- [87] H. du Mas des Bourboux *et al.*, The completed SDSS-IV
extended baryon oscillation spectroscopic survey: Baryon
acoustic oscillations with Ly α forests, *Astrophys. J.* **901**,
153 (2020).
- [88] N. Palanque-Delabrouille, C. Yèche, N. Schöneberg,
J. Lesgourgues, M. Walther, S. Chabanier, and E.
Armengaud, Hints, neutrino bounds and WDM constraints
from SDSS DR14 Lyman- α and Planck full-survey data,
J. Cosmol. Astropart. Phys. **04** (2020) 038.
- [89] E. van Uitert, B. Joachimi, S. Joudaki, A. Amon, C.
Heymans, F. Köhlinger, M. Asgari, C. Blake, A. Choi, T.
Erben *et al.*, KiDS + GAMA: Cosmology constraints from
a joint analysis of cosmic shear, galaxy–galaxy lensing,
and angular clustering, *Mon. Not. R. Astron. Soc.* **476**,
4662 (2018).
- [90] T. Hamana, M. Shirasaki, S. Miyazaki, C. Hikage,
M. Oguri, S. More, R. Armstrong, A. Leauthaud, R.
Mandelbaum, H. Miyatake *et al.*, Cosmological constraints
from cosmic shear two-point correlation functions with
HSC survey first-year data, *Publ. Astron. Soc. Jpn.* **72**, 16
(2020).
- [91] G. F. R. Ellis, R. Maartens, and M. A. H. MacCallum,
Relativistic Cosmology (Cambridge University Press,
Cambridge, England, 2012).
- [92] S. M. Carroll, M. Hoffman, and M. Trodden, Can the dark
energy equation-of-state parameter w be less than -1 ?,
Phys. Rev. D **68**, 023509 (2003).
- [93] E. J. Copeland, M. Sami, and S. Tsujikawa, Dynamics of
dark energy, *Int. J. Mod. Phys. D* **15**, 1753 (2006).
- [94] J. M. Maldacena, The Large N limit of superconformal
field theories and supergravity, *Adv. Theor. Math. Phys.* **2**,
231 (1998).
- [95] R. Bousso and J. Polchinski, Quantization of four form
fluxes and dynamical neutralization of the cosmological
constant, *J. High Energy Phys.* **06** (2000) 006.
- [96] J. M. Maldacena and C. Nunez, Supergravity description
of field theories on curved manifolds and a no go theorem,
Int. J. Mod. Phys. A **16**, 822 (2001).
- [97] S. Kachru, R. Kallosh, A. D. Linde, and S. P. Trivedi, De
Sitter vacua in string theory, *Phys. Rev. D* **68**, 046005
(2003).
- [98] N. Goheer, M. Kleban, and L. Susskind, The trouble with
de Sitter space, *J. High Energy Phys.* **07** (2003) 056.
- [99] H. Ooguri and C. Vafa, On the geometry of the string
landscape and the swampland, *Nucl. Phys.* **B766**, 21
(2007).
- [100] J. P. Conlon and F. Quevedo, Astrophysical and cosmo-
logical implications of large volume string compactifica-
tions, *J. Cosmol. Astropart. Phys.* **08** (2007) 019.
- [101] U. H. Danielsson and T. Van Riet, What if string theory has
no de Sitter vacua?, *Int. J. Mod. Phys. D* **27**, 1830007 (2018).
- [102] E. Witten, Quantum gravity in de Sitter space, [arXiv:hep-
th/0106109](https://arxiv.org/abs/hep-th/0106109).
- [103] K. Dutta and A. Maharana, Models of accelerating uni-
verse in supergravity and string theory, *Eur. Phys. J.*
Special Topics **230**, 2111 (2021).
- [104] Y. S. Piao, Can the universe experience many cycles with
different vacua?, *Phys. Rev. D* **70**, 101302 (2004).

- 1780 [105] H. H. Li, G. Ye, Y. Cai, and Y. S. Piao, Trans-Planckian
1781 censorship of multistage inflation and dark energy, *Phys.*
1782 *Rev. D* **101**, 063527 (2020).
- 1783 [106] J. A. Vázquez, L. E. Padilla, and T. Matos, Inflationary
1784 cosmology: From theory to observations, *Rev. Mex. Fis. E.*
1785 **17**, 31349 (2019).
- 1786 [107] W. Yin, Small cosmological constant from a peculiar
1787 inflaton potential, [arXiv:2108.04246](https://arxiv.org/abs/2108.04246).
- 1788 [108] V. Faraoni, E. Gunzig, and P. Nardone, Conformal trans-
1789 formations in classical gravitational theories and in cos-
1790 mology, *Fundam. Cosm. Phys.* **20**, 121 (1999).
- 1791 [109] B. Boisseau, G. Esposito-Farese, D. Polarski, and A. A.
1792 Starobinsky, Reconstruction of a Scalar-Tensor Theory of
1793 Gravity in an Accelerating Universe, *Phys. Rev. Lett.* **85**,
1794 2236 (2000).
- 1795 [110] V. Sahni and A. Starobinsky, Reconstructing dark energy,
1796 *Int. J. Mod. Phys. D* **15**, 2105 (2006).
- 1797 [111] Ö. Akarsu, N. Katırcı, N. Özdemir, and J. A. Vazquez,
1798 Anisotropic massive Brans-Dicke gravity extension of
1799 standard Λ CDM model, *Eur. Phys. J. C* **80**, 32 (2020).
- 1800 [112] J. Solà Peracaula, A. Gómez-Valent, J. de Cruz Pérez,
1801 and C. Moreno-Pulido, Brans–Dicke cosmology with a
1802 Λ -term: A possible solution to Λ CDM tensions, *Classical*
1803 *Quantum Gravity* **37**, 245003 (2020).
- 1804 [113] T. Harko and F. S. N. Lobo, $f(R, \mathcal{L}_m)$ gravity, *Eur. Phys. J.*
1805 *C* **70**, 373 (2010).
- 1806 [114] T. Harko, F. S. N. Lobo, S. Nojiri, and S. D. Odintsov,
1807 $f(R, T)$ gravity, *Phys. Rev. D* **84**, 024020 (2011).
- 1808 [115] N. Katırcı and M. Kavuk, $f(R, T_{\mu\nu} T^{\mu\nu})$ gravity and
1809 Cardassian-like expansion as one of its consequences,
1810 *Eur. Phys. J. Plus* **129**, 163 (2014).
- 1811 [116] M. Roshan and F. Shojai, Energy-momentum squared
1812 gravity, *Phys. Rev. D* **94**, 044002 (2016).
- 1813 [117] Ö. Akarsu, N. Katırcı, and S. Kumar, Cosmic acceleration
1814 in a dust only Universe via energy-momentum powered
1815 gravity, *Phys. Rev. D* **97**, 024011 (2018).
- 1816 [118] C. V. R. Board and J. D. Barrow, Cosmological models in
1817 energy-momentum-squared gravity, *Phys. Rev. D* **96**,
1818 123517 (2017).
- 1819 [119] Ö. Akarsu, N. Katırcı, S. Kumar, R. C. Nunes, and M.
1820 Sami, Cosmological implications of scale-independent
1821 energy-momentum squared gravity: Pseudo nonminimal
1822 interactions in dark matter and relativistic relics, *Phys. Rev.*
1823 *D* **98**, 063522 (2018).
- 1824 [120] Ö. Akarsu, J. D. Barrow, C. V. R. Board, N. M. Uzun, and
1825 J. A. Vazquez, Screening Λ in a new modified gravity
1826 model, *Eur. Phys. J. C* **79**, 846 (2019).
- 1827 [121] A. D. Dolgov, Field model with a dynamic cancellation of
1828 the cosmological constant, *JETP Lett.* **41**, 345 (1985).
- 1829 [122] A. D. Dolgov, Field model with a dynamic cancellation of
1830 the cosmological constant, *Pis'ma Zh. Eksp. Teor. Fiz.* **41**,
1831 280 (1985).
- 1832 [123] F. Bauer, J. Sola, and H. Stefancic, Dynamically avoiding
1833 fine-tuning the cosmological constant: The 'Relaxed Uni-
1834 verse', *J. Cosmol. Astropart. Phys.* **12** (2010) 029.
- 1835 [124] S. Y. Zhou, E. J. Copeland, and P. M. Saffin, Cosmological
1836 constraints on $f(G)$ dark energy models, *J. Cosmol.*
1837 *Astropart. Phys.* **07** (2009) 009.
- 1838 [125] V. Sahni and Y. Shtanov, Braneworld models of dark
1839 energy, *J. Cosmol. Astropart. Phys.* **11** (2003) 014.
- [126] P. Brax and C. van de Bruck, Cosmology and brane 1840
worlds: A review, *Classical Quantum Gravity* **20**, R201 1841
(2003). 1842
- [127] A. Chodos and S. L. Detweiler, Where has the fifth- 1843
dimension gone?, *Phys. Rev. D* **21**, 2167 (1980). 1844
- [128] T. Dereli and R. W. Tucker, Dynamical reduction of 1845
internal dimensions in the early Universe, *Phys. Lett.* 1846
125B, 133 (1983). 1847
- [129] Ö. Akarsu and T. Dereli, The dynamical evolution of 1848
3-space in a higher dimensional steady state Universe, 1849
Gen. Relativ. Gravit. **45**, 959 (2013). 1850
- [130] Ö. Akarsu and T. Dereli, Late time acceleration of the 1851
3-space in a higher dimensional steady state Universe in 1852
dilatón gravity, *J. Cosmol. Astropart. Phys.* **02** (2013) 050. 1853
- [131] J. G. Russo and P. K. Townsend, Late-time cosmic accel- 1854
eration from compactification, *Classical Quantum Gravity* 1855
36, 095008 (2019). 1856
- [132] B. Boisseau, H. Giacomini, D. Polarski, and A. A. 1857
Starobinsky, Bouncing Universes in scalar-tensor gravity 1858
models admitting negative potentials, *J. Cosmol. Astro-* 1859
part. Phys. **07** (2015) 002. 1860
- [133] J. Grande, J. Sola, and H. Stefancic, Λ XCDM: A Cosmon 1861
model solution to the cosmological coincidence problem?, 1862
J. Cosmol. Astropart. Phys. **08** (2006) 011. 1863
- [134] M. Bouhmadi-Lopez, A. Errahmani, P. Martin-Moruno, T. 1864
Ouali, and Y. Tavakoli, The little sibling of the big rip 1865
singularity, *Int. J. Mod. Phys. D* **24**, 1550078 (2015). 1866
- [135] J. D. Barrow, Graduated inflationary Universes, *Phys. Lett.* 1867
B 235, 40 (1990). 1868
- [136] H. Stefancic, Expansion around the vacuum equation of 1869
state—Sudden future singularities and asymptotic behav- 1870
ior, *Phys. Rev. D* **71**, 084024 (2005). 1871
- [137] J. P. Petit and G. d'Agostini, Negative mass hypothesis in 55 1872
cosmology and the nature of dark energy, *Astrophys.* 1873
Space Sci. **354**, 611 (2014). 1874
- [138] J. S. Farnes, A unifying theory of dark energy and dark 1875
matter: Negative masses and matter creation within a 1876
modified Λ CDM framework, *Astron. Astrophys.* **620**, 1877
A92 (2018). 1878
- [139] S. Nájera, A. Gamboa, A. Aguilar-Nieto, and C. Escamilla- 1879
Rivera, On negative mass cosmology in general relativity, 1880
Astron. Astrophys. **651**, L13 (2021). 1881
- [140] A. Chavda, J. D. Barrow, and C. G. Tsagas, Kinematical 1882
and dynamical aspects of ghost-matter cosmologies, 1883
Classical Quantum Gravity **37**, 205010 (2020). 1884
- [141] D. J. Fixsen, The temperature of the cosmic microwave 1885
background, *Astrophys. J.* **707**, 916 (2009). 1886
- [142] Ø. Grøn and S. Hervik, *Einstein's General Theory of* 1887
Relativity: With Modern Applications in Cosmology 1888
(Springer-Verlag, New York, 2007). 1889
- [143] J. L. Bernal, L. Verde, and A. G. Riess, The trouble with 1890
 H_0 , *J. Cosmol. Astropart. Phys.* **10** (2016) 019. 1891
- [144] K. Aylor, M. Joy, L. Knox, M. Millea, S. Raghunathan, and 1892
W. L. K. Wu, Sounds discordant: Classical distance ladder 1893
& Λ CDM -based determinations of the cosmological 1894
sound horizon, *Astrophys. J.* **874**, 4 (2019). 1895
- [145] G. Efstathiou, To H_0 or not to H_0 ?, *Mon. Not. R. Astron.* 1896
Soc. **505**, 3866 (2021). 1897
- [146] D. Camarena and V. Marra, On the use of the local prior on 1898
the absolute magnitude of Type Ia supernovae in cosmo- 1899

- logical inference, *Mon. Not. R. Astron. Soc.* **504**, 5164 (2021).
- [147] D. Camarena and V. Marra, Local determination of the Hubble constant and the deceleration parameter, *Phys. Rev. Research* **2**, 013028 (2020).
- [148] L. Anderson *et al.* (BOSS Collaboration), The clustering of galaxies in the SDSS-III baryon oscillation spectroscopic survey: Baryon acoustic oscillations in the data releases 10 and 11 galaxy samples, *Mon. Not. R. Astron. Soc.* **441**, 24 (2014).
- [149] D. Camarena and V. Marra, A new method to build the (inverse) distance ladder, *Mon. Not. R. Astron. Soc.* **495**, 2630 (2020).
- [150] D. M. Scolnic, D. O. Jones, A. Rest, Y. C. Pan, R. Chornock, R. J. Foley, M. E. Huber, R. Kessler, G. Narayan, A. G. Riess *et al.*, The complete light-curve sample of spectroscopically confirmed SNe Ia from Pan-STARRS1 and cosmological constraints from the combined pantheon sample, *Astrophys. J.* **859**, 101 (2018).
- [151] P. Lemos, E. Lee, G. Efstathiou, and S. Gratton, Model independent $H(z)$ reconstruction using the cosmic inverse distance ladder, *Mon. Not. R. Astron. Soc.* **483**, 4803 (2019).
- [152] G. Benevento, W. Hu, and M. Raveri, Can late dark energy transitions raise the Hubble constant?, *Phys. Rev. D* **101**, 103517 (2020).
- [153] A. De Felice, S. Mukohyama, and M. C. Pookkillath, Addressing H_0 tension by means of Λ CDM, *Phys. Lett. B* **816**, 136201 (2021).
- [154] G. Alestas and L. Perivolaropoulos, Late-time approaches to the Hubble tension deforming $H(z)$, worsen the growth tension, *Mon. Not. R. Astron. Soc.* **504**, 3956 (2021).
- [155] R. C. Nunes and E. Di Valentino, Dark sector interaction and the supernova absolute magnitude tension, *Phys. Rev. D* **104**, 063529 (2021).
- [156] G. Alestas, L. Kazantzidis, and L. Perivolaropoulos, $w - M$ phantom transition at $z_t < 0.1$ as a resolution of the Hubble tension, *Phys. Rev. D* **103**, 083517 (2021).
- [157] V. Marra and L. Perivolaropoulos, Rapid transition of G_{eff} at $z_t \simeq 0.01$ as a possible solution of the Hubble and growth tensions, *Phys. Rev. D* **104**, L021303 (2021).
- [158] L. Perivolaropoulos and F. Skara, Hubble tension or a transition of the Cepheid SNIa calibrator parameters?, [arXiv:2109.04406](https://arxiv.org/abs/2109.04406).
- [159] A. Theodoropoulos and L. Perivolaropoulos, The Hubble tension, the M crisis of late time $H(z)$ deformation models and the reconstruction of quintessence lagrangians, *Universe* **7**, 300 (2021).
- [160] N. Aghanim *et al.* (Planck Collaboration), *Planck* 2018 results. VIII. Gravitational lensing, *Astron. Astrophys.* **641**, A8 (2020).
- [161] M. Ata *et al.*, The clustering of the SDSS-IV extended baryon oscillation spectroscopic survey DR14 quasar sample: First measurement of baryon acoustic oscillations between redshift 0.8 and 2.2, *Mon. Not. R. Astron. Soc.* **473**, 4773 (2018).
- [162] F. Beutler, C. Blake, M. Colless, D. H. Jones, L. Staveley-Smith, L. Campbell, Q. Parker, W. Saunders, and F. Watson, The 6dF galaxy survey: Baryon acoustic oscillations and the local Hubble constant, *Mon. Not. R. Astron. Soc.* **416**, 3017 (2011).
- [163] A. Lewis and S. Bridle, Cosmological parameters from CMB and other data: A Monte Carlo approach, *Phys. Rev. D* **66**, 103511 (2002).
- [164] MCEvidence is publicly available online at <https://github.com/yabebalFantaye/MCEvidence>.
- [165] J. A. Vazquez, A. N. Lasenby, M. Bridges, and M. P. Hobson, A Bayesian study of the primordial power spectrum from a novel closed universe model, *Mon. Not. R. Astron. Soc.* **422**, 1948 (2012).
- [166] L. E. Padilla, L. O. Tellez, L. A. Escamilla, and J. A. Vazquez, Cosmological parameter inference with Bayesian statistics, *Universe* **7**, 213 (2021).
- [167] R. J. Cooke, M. Pettini, and C. C. Steidel, One percent determination of the primordial deuterium abundance, *Astrophys. J.* **855**, 102 (2018).
- [168] L. E. Marcucci, G. Mangano, A. Kievsky, and M. Viviani, Implication of the proton-deuteron radiative capture for Big Bang Nucleosynthesis, *Phys. Rev. Lett.* **116**, 102501 (2016); Erratum, *Phys. Rev. Lett.* **117**, 049901 (2016).
- [169] E. G. Adelberger, A. B. Balantekin, D. Bemmerer, C. A. Bertulani, J. W. Chen, H. Costantini, M. Couder, R. Cyburt, B. Davids, S. J. Freedman *et al.*, Solar fusion cross sections II: The pp chain and CNO cycles, *Rev. Mod. Phys.* **83**, 195 (2011).
- [170] W. Handley, fgivenx: A Python package for functional posterior plotting, *J. Open Source Software* **3**, 849 (2018).
- [171] C. Heymans, T. Tröster, M. Asgari, C. Blake, H. Hildebrandt, B. Joachimi, K. Kuijken, C. A. Lin, A. G. Sánchez, J. L. van den Busch *et al.*, KiDS-1000 cosmology: Multi-probe weak gravitational lensing and spectroscopic galaxy clustering constraints, *Astron. Astrophys.* **646**, A140 (2021).
- [172] T. M. C. Abbott *et al.* (DES Collaboration), Dark energy survey year 3 results: Cosmological constraints from galaxy clustering and weak lensing, [arXiv:2105.13549](https://arxiv.org/abs/2105.13549).
- [173] Y. Akrami *et al.* (Planck Collaboration), *Planck* 2018 results. X. Constraints on inflation, *Astron. Astrophys.* **641**, A10 (2020).
- [174] R. Trotta, Bayes in the sky: Bayesian inference and model selection in cosmology, *Contemp. Phys.* **49**, 71 (2008).
- [175] R. Trotta, Bayesian methods in cosmology, [arXiv:1701.01467](https://arxiv.org/abs/1701.01467).
- [176] R. E. Kass and A. E. Raftery, Bayes factors, *J. Am. Stat. Assoc.* **90**, 773 (1995).
- [177] G. F. R. Ellis, H. van Elst, J. Murugan, and J. P. Uzan, On the trace-free einstein equations as a viable alternative to general relativity, *Classical Quantum Gravity* **28**, 225007 (2011).
- [178] T. Josset, A. Perez, and D. Sudarsky, Dark Energy from Violation of Energy Conservation, *Phys. Rev. Lett.* **118**, 021102 (2017).
- [179] A. Perez and D. Sudarsky, Dark Energy from Quantum Gravity Discreteness, *Phys. Rev. Lett.* **122**, 221302 (2019).
- [180] A. Perez, D. Sudarsky, and J. D. Bjorken, A microscopic model for an emergent cosmological constant, *Int. J. Mod. Phys. D* **27**, 1846002 (2018).

- 2018 [181] A. Perez and D. Sudarsky, Black holes, Planckian
2019 granularity, and the changing cosmological constant',
2020 *Gen. Relativ. Gravit.* **53**, 40 (2021).
2021 [182] Ö. Akarsu, S. Kumar, E. Özülker, and J. A. Vazquez,
2022 Relaxing the H_0 tension with diffusion à la unimodular
2023 gravity (to be published).
2024 [183] M. Ahmed, S. Dodelson, P. B. Greene, and R. Sorkin,
2025 Everpresent Λ , *Phys. Rev. D* **69**, 103523 (2004).
2026 [184] N. Zwane, N. Afshordi, and R. D. Sorkin, Cosmological
2027 tests of everpresent Λ , *Classical Quantum Gravity* **35**,
2028 194002 (2018).
2029 [185] S. Surya, The causal set approach to quantum gravity,
2030 *Living Rev. Relativity* **22**, 5 (2019).
2031 [186] A. Mazumdar and G. White, Review of cosmic phase
2032 transitions: Their significance and experimental signatures,
2033 *Rep. Prog. Phys.* **82**, 076901 (2019).
2034 [187] K. Sato, First order phase transition of a vacuum and
2035 expansion of the Universe, *Mon. Not. R. Astron. Soc.* **195**,
2036 467 (1981).
2037 [188] R. Kallosh, A. D. Linde, S. Prokushkin, and M. Shmakova,
2038 Gauged supergravities, de Sitter space and cosmology,
2039 *Phys. Rev. D* **65**, 105016 (2002).
2040 [189] R. Kallosh and A. D. Linde, M theory, cosmological
2041 constant and anthropic principle, *Phys. Rev. D* **67**,
2042 023510 (2003).
2043 [190] J. Garriga and A. Vilenkin, Testable anthropic predictions
2044 for dark energy, *Phys. Rev. D* **67**, 043503 (2003).
2045 [191] J. Garriga, A. D. Linde, and A. Vilenkin, Dark energy
2046 equation of state and anthropic selection, *Phys. Rev. D* **69**,
2047 063521 (2004).
2048 [192] R. R. Caldwell, W. Komp, L. Parker, and D. A. T. Vanzella,
2049 A sudden gravitational transition, *Phys. Rev. D* **73**, 023513
2050 (2006).
2051 [193] J. Polchinski, The cosmological constant and the string
2052 landscape, [arXiv:hep-th/0603249](https://arxiv.org/abs/hep-th/0603249).
2053 [194] W. Kim and M. Yoon, Transition from AdS universe to DS
2054 universe in the BPP model, *J. High Energy Phys.* **04** (2007)
2055 098.
2056 [195] T. Biswas and A. Mazumdar, Inflation with a negative
2057 cosmological constant, *Phys. Rev. D* **80**, 023519 (2009).
2058 [196] T. Prokopec, Negative energy cosmology and the cosmo-
2059 logical constant, [arXiv:1105.0078](https://arxiv.org/abs/1105.0078).
2060 [197] X. Dong, B. Horn, S. Matsuura, E. Silverstein, and
2061 G. Torroba, FRW solutions and holography from uplifted
2062 AdS/CFT, *Phys. Rev. D* **85**, 104035 (2012).
2063 [198] B. Gupt and P. Singh, Nonsingular AdS-dS transitions in a
2064 landscape scenario, *Phys. Rev. D* **89**, 063520 (2014).
2065 [199] M. Cadoni and M. Ciulu, Dark energy from holographic
2066 theories with hyperscaling violation, *J. High Energy Phys.*
2067 **05** (2014) 089.
- [200] X. O. Camanho, J. D. Edelstein, G. Giribet, and A. 2068
Gomberoff, Generalized phase transitions in Lovelock 2069
gravity, *Phys. Rev. D* **90**, 064028 (2014). 2070
- [201] X. O. Camanho, J. D. Edelstein, A. Gomberoff, and J. A. 2071
Sierra-Garcia, On AdS to dS transitions in higher- 2072
curvature gravity, *J. High Energy Phys.* **10** (2015) 179. 2073
- [202] Y. Akrami, R. Kallosh, A. Linde, and V. Vardanyan, 2074
Dark energy, α -attractors, and large-scale structure sur- 2075
veys, *J. Cosmol. Astropart. Phys.* **06** (2018) 041. 2076
- [203] S. Banerjee, U. Danielsson, G. Dibitetto, S. Giri, and M. 2077
Schillo, Emergent de Sitter Cosmology from Decaying 2078
Anti-de Sitter Space, *Phys. Rev. Lett.* **121**, 261301 (2018). 2079
- [204] F. Denef, A. Hebecker, and T. Wrase, de Sitter swampland 2080
conjecture and the Higgs potential, *Phys. Rev. D* **98**,
2081 086004 (2018). 2082
- [205] S. Kachru and S. P. Trivedi, A comment on effective field 2083
theories of flux vacua, *Fortschr. Phys.* **67**, 1800086 (2019). 2084
- [206] J. J. Heckman, C. Lawrie, L. Lin, and G. Zoccarato, 2085
F-theory and dark energy, *Fortschr. Phys.* **67**, 1900057
2086 (2019). 2087
- [207] E. Kiritsis and A. Tsouros, de Sitter versus anti de Sitter 2088
flows and the (super)gravity landscape, [arXiv:1901.04546](https://arxiv.org/abs/1901.04546). 2089
- [208] J. J. Heckman, C. Lawrie, L. Lin, J. Sakstein, and G. 2090
Zoccarato, Pixelated dark energy, *Fortschr. Phys.* **67**,
2091 1900071 (2019). 2092
- [209] P. Berglund, T. Hübsch, and D. Minic, On stringy de Sitter 2093
spacetimes, *J. High Energy Phys.* **12** (2019) 166. 2094
- [210] P. Berglund, T. Hübsch, and D. Minić, Dark energy and 2095
string theory, *Phys. Lett. B* **798**, 134950 (2019). 2096
- [211] S. Banerjee, U. Danielsson, G. Dibitetto, S. Giri, and M. 2097
Schillo, de Sitter cosmology on an expanding bubble,
2098 *J. High Energy Phys.* **10** (2019) 164. 2099
- [212] S. P. De Alwis, F. Muia, V. Pasquarella, and F. Quevedo, 2100
Quantum transitions between minkowski and de Sitter
2101 spacetimes, *Fortschr. Phys.* **68**, 2000069 (2020). 2102
- [213] S. A. Franchino-Viñas and S. Mignemi, Asymptotic free- 2103
dom for $\lambda\phi^4$ QFT in Snyder-de Sitter space, *Eur. Phys. J.*
2104 **C 80**, 382 (2020). 2105
- [214] D. Samart and P. Channuaie, Gravitational AdS to dS phase 2106
transition in five-dimensional Einstein-Maxwell-Gauss-
2107 Bonnet gravity, *Phys. Rev. D* **102**, 064008 (2020). 2108
- [215] D. Samart and P. Channuaie, Gravitational phase transition 2109
mediated by thermalon in Einstein-Gauss-Bonnet-
2110 Maxwell-Kalb-Ramond gravity, *J. High Energy Phys.*
2111 **08** (2020) 100. 2112
- [216] D. Samart and P. Channuaie, AdS to dS phase transition 2113
mediated by thermalon in Einstein-Gauss-Bonnet gravity
2114 from Rényi statistics, [arXiv:2012.14828](https://arxiv.org/abs/2012.14828). 2115
- [217] P. Berglund, T. Hübsch, and D. Minic, Stringy bubbles 2116
solve de Sitter troubles, *Universe* **7**, 363 (2021). 2117
2118